Chapter 5

Synthesis of Gallium(III) Pentacoordinated Complexes

5.1 Gallium pentacoordinated complexes with phenols

The literature report pentacoordinated gallium(III) compounds, with the general formula Q'_2GaL, obtained with two equivalent of 2-methyl-8-hydroxyquinoline (HQ') and one equivalent of a monodentate ligand (HL) as phenols, carboxylic acids an halides.[1-6] The synthesis of new pentacoordinated gallium complexes was performed adapting the method suggested by Sapochak *et al.*.[1] Compounds of the general formula $\mathbf{Q'_2GaL^n}$ were obtained with two equivalent of 2-methyl-8-hydroxyquinoline and one equivalent of a monodentate ligand (HL^n) as a phenol and its *p*-substituted derivatives as *p*-cyanophenol and *p*-nitrophenol (**Figure 5.1**).

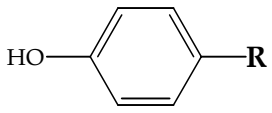

HL^1 **R=** -H

HL^2 -CN

HL^3 -NO_2

Figure 5.1: *p-substituted phenols (HL^n).*

In order to avoid the competitive formation of the hexacoordinated tris-chelated GaQ'_3 derivative, the phenol ligands were activated by sodium hydroxide in ethanol, as described in **Scheme 5.1**, prior to be added to the reaction mixture

containing gallium(III) nitrate hydrate salt dissolved in a considerable amount of water to control the reaction mixture acidity.

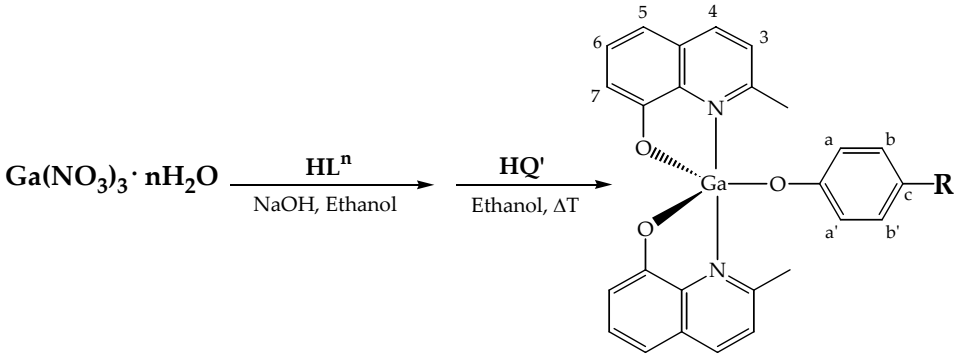

HL[1]	phenol	**R=** -H	**Q'$_2$GaOC$_6$H$_5$**
HL[2]	*p*-cyanophenol	-CN	**Q'$_2$GaOC$_6$H$_4$CN**
HL[3]	*p*-nitrophenol	-NO_2	**Q'$_2$GaOC$_6$H$_4$NO$_2$**

HQ' = 2-methyl-8-hydroxyquinoline

Scheme 5.1: *synthesis of bis(2-methyl-8-hydroxyquinolinate) gallium(III) phenolate.*

The desired compounds: **Q′$_2$GaOC$_6$H$_5$**, **Q′$_2$GaOC$_6$H$_4$CN** and **Q′$_2$GaOC$_6$H$_4$NO$_2$**; were obtained as greenish yellow crystalline powders in relatively good overall yield. All compounds show high solubility in chloroform. The complexes were characterized by elemental analysis, IR, ^{1}H NMR spectroscopy, X-ray diffraction on single crystal, differential scanning calorimetry (DSC) and cyclic voltammetry (CV). The infrared spectra show characteristic C–H stretching bands of the methyl group ranging from 3000 and 3100 cm^{-1}, further the typical bands of the coordinated Q′ fragment in the 1610 - 1110 cm^{-1} range; in the case of **Q′$_2$GaOC$_6$H$_4$CN** the stretching band relative to the –CN group is observed at 2221 cm^{-1}, while for **Q′$_2$GaOC$_6$H$_4$NO$_2$** the intense band at 1303 cm^{-1} is ascribed to the stretching of the –NO_2 group. The ^{1}H NMR spectra of all compounds, collected in deuterated chloroform, are consistent with the proposed structures, revealing the magnetic equivalence of the two Q′ moieties with only one set of signals, slightly shifted to higher frequencies when the phenol ligand is *p*-

substituted. The chemical shift of the $H^{a,a'}$ and $H^{b,b'}$ signals, corresponding to the hydrogens of the phenol ring is weakly influenced by the presence of the gallium centre. In all cases a weak shield to lower frequencies can be observed with respect to the corresponding ligand. In **Figure 5.2** are reported the ^1H NMR spectra of **Q′$_2$GaL^n** compounds.

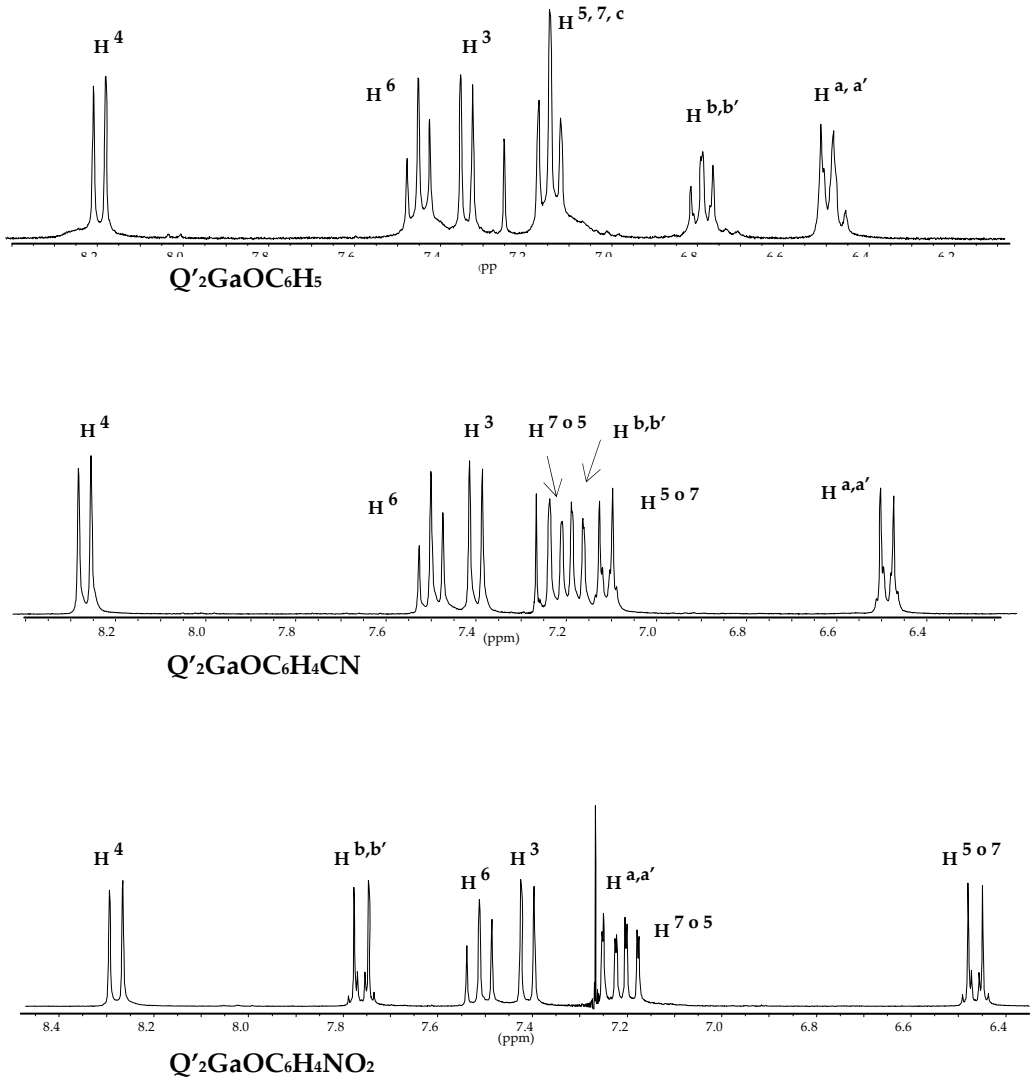

Figure 5.2: *^1H NMR of* ***Q′$_2$GaOC$_6$H$_5$, Q′$_2$GaOC$_6$H$_4$CN*** *and* ***Q′$_2$GaOC$_6$H$_4$NO$_2$.***

The redox potentials were measured versus ferrocene as internal references (Cp_2Fe/Cp_2Fe^+) using tetrabutylammonium perfluorate (0.1M) as electrolyte in dichloromethane-acetonitrile (1:1) solutions. CV analyses showed no reduction

waves for all complexes inside the solvent window. Oxidation processes have been noticed as broad irreversible waves above 1300 mV. The non well-defined irreversible oxidation waves and the precipitation at the Pt working electrode surface prevent further analysis. All microcrystalline complexes were thermally characterized by DSC analysis. In all cases the trace show only high melting peak values. The **Figure 5.3** shows the behaviour of **Q'$_2$GaOC$_6$H$_4$CN**. This graph represent an example of the thermal behaviour of this series of compounds. So as can be observed any polymorphism depending on the temperature was noticed.

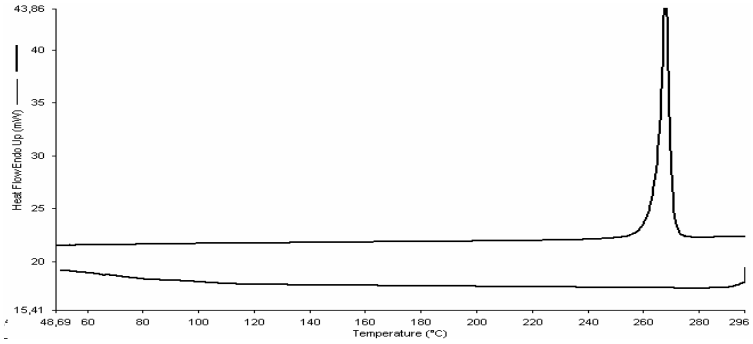

***Figure 5.3: Q'$_2$GaOC$_6$H$_4$CN** DSC graph.*

The possible generation of a glassy state is an interesting feature of these materials. Because of the morphological stability is one of the important requirements of the amorphous thin film in order to be exploited in OLED technologies. Further, the high melting point, above 250 °C, is another important requirement for this kind of applications due to the temperatures generated into the thin film, as Joule effect, during the current flow.

Stability tests were collected following the method described in Chapter 4.

A dichloromethane solution, 1x10^{-4} M, of **Q'$_2$GaL^n** compounds was dropped to a cuvette containing cyclohexane. Then each of the thirty additions was followed by collection of absorption spectra. The ratio of the absorption maximum at 245

nm and at 260 nm, $\mathbf{A_{245}/A_{260}}$, respectively, were plotted versus the timescale. **Figure 5.4** report the absorption spectra and the $\mathbf{A_{245}/A_{260}}$ ratio values. When the absorption band at 245 nm grows in intensity the $\mathbf{A_{245}/A_{260}}$ ratio value increase.

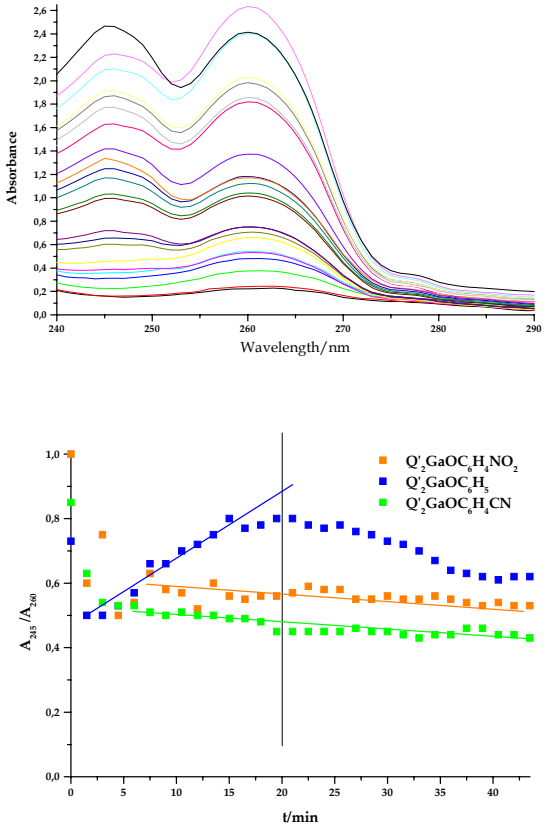

Figure 5.4: *chemical stability in cyclohexane solvent.*

The ratio value, in the case of $\mathbf{Q'_2GaOC_6H_5}$, achieve a maximum after twenty added drops, then the ratio value start to decrease. This behaviour is due to the fact that the absorption band at 260 nm shows very high intensity, so after a certain number of added drops the concentration is to high to detect some change in the absorption profile. The plotted graphs report a stable chemical behaviour of $\mathbf{Q'_2GaOC_6H_4CN}$ and $\mathbf{Q'_2GaOC_6H_4NO_2}$, in the forced chemical environment previously described, and a certain lability of $\mathbf{Q'_2GaOC_6H_5}$ compound.

5.1.1 Structural features of $Q'_2GaOC_6H_5$, $Q'_2GaOC_6H_4CN$ and $Q'_2GaOC_6H_4NO_2$

Molecular structure of **$Q'_2GaOC_6H_5$**, **$Q'_2GaOC_6H_4CN$** and **$Q'_2GaOC_6H_4NO_2$** complexes has been obtained through single crystal X-ray diffraction analysis performed on good quality crystals obtained in all cases from slow diffusion of *n*-hexane in a chloroform solution. Complex **$Q'_2GaOC_6H_5$** is monoclinic, crystallizing in the $P2_1/c$ space group while both **$Q'_2GaOC_6H_4CN$** and **$Q'_2GaOC_6H_4NO_2$** compounds crystallize in the triclinic space group *P*-1 with almost the same cell parameters. The perspective drawing of complex **$Q'_2GaOC_6H_5$** is illustrated in **Figure 5.5** while those of complexes **$Q'_2GaOC_6H_4CN$** and **$Q'_2GaOC_6H_4NO_2$** are reported in **Figure 5.6**.

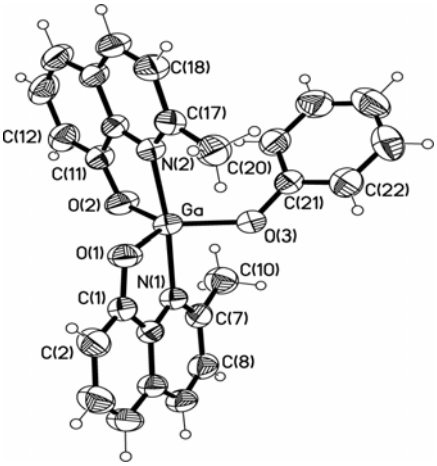

Figure 5.5: *perspective drawing of $Q'_2GaOC_6H_5$ complex.*

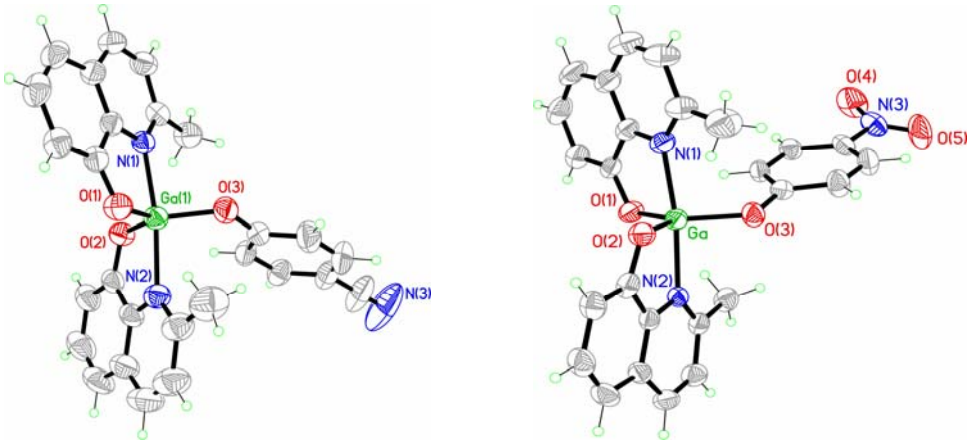

Figure 5.6: *perspective drawing of **$Q'_2GaOC_6H_4CN$** and **$Q'_2GaOC_6H_4NO_2$** complexes.*

The crystallographic data of all compounds are reported in the **Table 5.1**.

Q'_2GaL^n	**$Q'_2GaOC_6H_5$,**	**$Q'_2GaOC_6H_5$,**	**$Q'_2GaOC_6H_5$,**
fw	479.17	504.18	524.17
Crystal System	monoclinic	triclinic	triclinic
space group	$P2_1/c$	P -1	P -1
a , Å	15.736(1)	9.199(2)	9.077(2)
b , Å	10.9021(8)	9.670(2)	9.410(2)
c , Å	13.209(1)	15.109(3)	15.134(3)
α, deg	90	106.774(4)	105.23(3)
β, deg	103.836(3)	91.538(4)	92.54(3)
γ, deg	90	114.381(3)	113.09(3)
V, Å^3	2200.2(3)	1155.5(4)	1131.4(4)
Z	4	2	2
D(calcd), g/cm^3	1.447	1.449	1.539
μ, mm^{-1}	1.281	1.225	1.261
temp, K	298	298	298
F(000)	984	516	536
θ(deg)	2.29 to 30.51	1.43 to 24.71	2.44 to 25.05
no. measured reflns	55913	10323	4286
no. unique reflns	6727 [R(int) = 0.0345]	3933 [R(int)= 0.0164]	4009 [R(int)= 0.0314]
reflns with $I > \theta(I)$	4990	3628	3043
refined params	291	308	316
goodness-of-fit	1.026	1.109	1.035
R indices, [a, b]	$R1$ = 0.0361, $wR2$= 0.0932	$R1$ = 0.0269, $wR2$= 0.0762	$R1$ = 0.0450, $wR2$= 0.1083
R indices (all data)	$R1$ = 0.0544, $wR2$= 0.1052	$R1$ = 0.0291, $wR2$= 0.0798	$R1$ = 0.0603, $wR2$= 0.1124

[a] $R1 = \sum(||F_o| - |F_c||)/\sum|F_o|$. [b] $wR2 = [\sum w(F_o^2 - F_c^2)^2 / \sum w(F_o^2)^2]^{1/2}$.

Table 5.1: *crystallographic data .*

Table 5.2 report the selected bond distances and angles of **Q′$_2$GaL^n** complexes.

Q′$_2$GaL^n	**Q′$_2$GaOC$_6$H$_5$,**	**Q′$_2$GaOC$_6$H$_4$CN**	**Q′$_2$GaOC$_6$H$_4$NO$_2$**
Ga-O(1)	1.885(1)	1.872(1)	1.868(2)
Ga-O(2)	1.881(1)	1.868(1)	1.872(3)
Ga-O(3)	1.852(1)	1.851(1)	1.863(3)
Ga-N(1)	2.084(2)	2.084(2)	2.081(3)
Ga-N(2)	2.091(1)	2.088(2)	2.077(3)
O(1)-Ga-O(2)	116.61(7)	119.18(7)	118.55(12)
O(1)-Ga-O(3)	117.54(7)	116.93(7)	117.85(12)
O(1)-Ga-N(1)	83.78(6)	83.77(6)	83.82(11)
O(1)-Ga-N(2)	91.48(6)	92.43(6)	91.89(12)
O(2)-Ga-O(3)	125.79(7)	123.88(7)	123.59(12)
O(2)-Ga-N(1)	94.25(6)	91.77(6)	92.82(12)
O(2)-Ga-N(2)	83.60(6)	83.66(7)	83.65(12)
N(1)-Ga-N(2)	173.28(6)	171.73(6)	172.35(12)

Table 5.2: *selected bond distances (Å) and angles (°).*

The angles around the Ga(III) ion approximate a trigonal bipyramid geometry, with the two Q′ ligands in an N,N *trans* conformation (N–Ga–N angle ranges from 171.4 to 173.3°). The average Ga–O and Ga–N bond distances are of 1.87 and 2.09 Å.

Intermolecular π–π stacking and hydrogen bonds interactions are the most remarkable structural features of the **Q′$_2$GaL^n** solids. An examination of the solid-state packing of all phenolate complexes shows that there are close intermolecular π–π stacking interactions mainly between the pyridyl–pyridyl rings of neighbouring molecules. The π–π stacking parameters and the operation symmetry are summarized in **Table 5.3**.

Q'_2GaL^n	[N(1)/C(9)]-[N(1)/C(9)] *	[N(2)/C(19)]-[N(2)/C(19)] *	[C(11)/C(16)]-[C(11)/C(16)] *	C–H---π
$Q'_2GaOC_6H_5$,	d [a] = 3.47 Å, [i] S [b] = 1.24 Å, α [c] = 19.7°	d = 3.46 Å, [ii] S = 0.92 Å, α = 14.9°		D = 2.90 Å, [v] C_{Ph}–H---X = 163.1°
$Q'_2GaOC_6H_4CN$	d = 3.43 Å, [iii] S = 0.98 Å, α = 16.4°	d = 3.55 Å, [i] S = 2.40 Å, α = 34.2°	d = 3.65 Å, [iv] S = 0.57 Å, α = 8.90°	D = 2.66 Å, [i] C_{Ph}–H---X = 162.6°
$Q'_2GaOC_6H_4NO_2$	d = 3.39 Å, [iii] S = 1.07 Å, α = 17.6°	d = 3.459Å, [i] S = 2.22 Å, α = 31.7°	d = 3.60 Å, [iv] S = 0.52 Å, α = 8.2°	D = 2.69 Å, [i] C_{Ph}–H---X = 158.7°

[a] *interplanar distance:* distance between the ring planes;
[b] *horizontal displacement:* distance between the ring normal and the centroid vector;
[c] *displacement angle:* angle between the ring normal and the centroid vector;
* *symmetry codes: (i)* 1–*x*, 2-*y*, 1-*z*; *(ii)* 2–*x*, 2-*y*, 1-*z*; *(iii)* 2–*x*, 2-*y*, 2-*z*; *(iv)* 1–*x*, 1-*y*, 1-*z*; *(v)* *x*, 1+*y*, *z*;

Table 5.3: *π–π stacking parameters of phenolate compounds.*

In all cases, both the Q′ ligands, nominally called the Q'_A (the N(1) quinolinate) and the Q'_B (the N(2) quinolinate) chelates, are involved in aromatic interactions with the symmetrical related rings, while stacks with mixed chelates are not found. The primary motif between the planar aromatic units for both chelates is the offset face-to-face (OFF) type, with the distance between the mean planes passing through the rings involved in the stacking within the range 3.3–3.8 Å, generally accepted for the phenomenon of π–π stacking. Moreover, the phenol rings are involved in edge-to-face interactions (EF), often referred as C–H–π hydrogen bonds, being the aromatic ring H donor in the case of complex $\mathbf{Q'_2GaOC_6H_5}$ and H acceptor in both complexes $\mathbf{Q'_2GaOC_6H_4CN}$ and $\mathbf{Q'_2GaOC_6H_4NO_2}$. While the Q'_A–Q'_A stacking is characterized by the same parameters in the series this gallium compounds, the Q'_B–Q'_B aromatic interaction differs from complex $\mathbf{Q'_2GaOC_6H_5}$ to complexes $\mathbf{Q'_2GaOC_6H_4CN}$ and $\mathbf{Q'_2GaOC_6H_4NO_2}$. The orthogonal views of the Q_A' (**a**) and the Q_B' (**b**) chelates stacking in complex $\mathbf{Q'_2GaOC_6H_5}$ are reported in **Figure 5.7**,

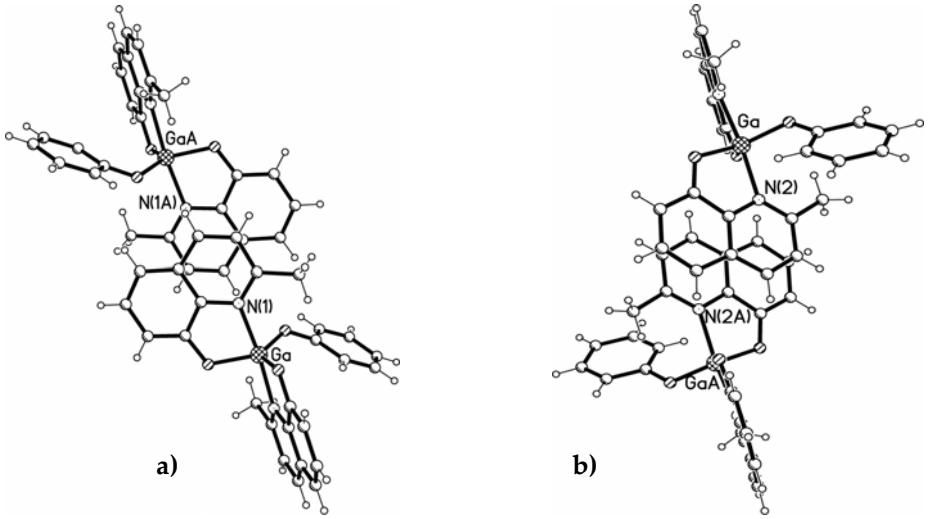

Figure 5.7: *orthogonal view of* Q_A' (***a***) *and* Q_B' (***b***) *chelates stacking in* $\mathbf{Q'_2GaOC_6H_5}$.

In fact, the Q'_B–Q'_B stacking in complex $\mathbf{Q'_2GaOC_6H_5}$ is characterized by a small transverse offset (less than 1 Å), which causes a nearly complete facing of the overall aromatic system, involving the pyridyl-fused phenolate rings in the same interaction as shown in **Figure 5.7**, drawing **b**. The crystal packing of complex $\mathbf{Q'_2GaOC_6H_5}$ reported in **Figure 5.8** shows in (**c**) the C–H---π hydrogen bonds between raw of molecules and in the drawing (**d**) the generation of secondary repetition motifs.

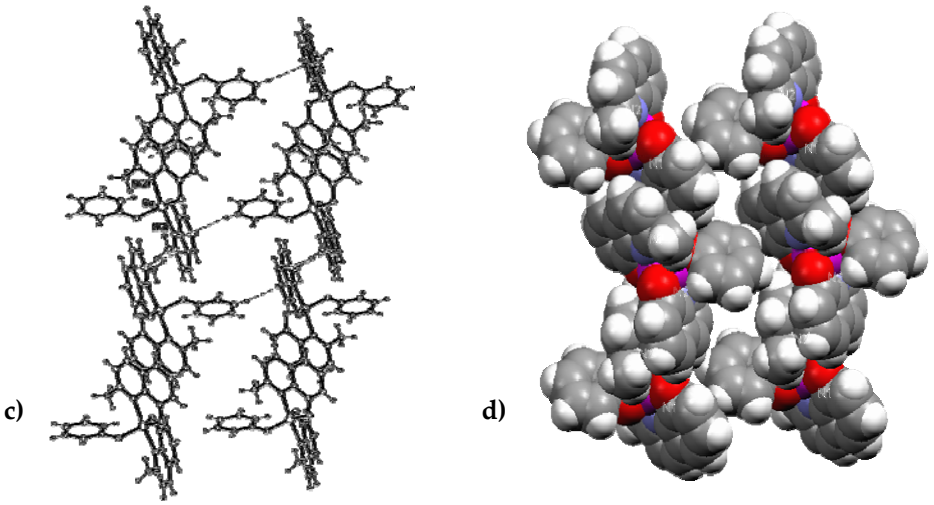

Figure 5.8: *C–H---π hydrogen bonds (**c**), secondary motif (**d**) of* $\mathbf{Q'_2GaOC_6H_5}$.

As previously described each molecule of **Q'$_2$GaOC$_6$H$_5$** interacts with two symmetrical related molecules through the Q'$_A$ and the Q'$_B$ chelates, generating extended two-dimensional chains illustrated in **Figure 5.8**, drawing **c**. Among chains, edge-to-face interactions occur between one hydrogen atom of the phenol ligand and the [C(1)/C(6)] aromatic ring of the Q'$_A$ chelate. Furthermore, the secondary repetition motif recognizable is a combination of two OFF and two EF interactions in **Figure 5.8**, drawing **d**.

The orthogonal views of the Q$_A$' (**a**) and the Q$_B$' (**b**) chelates stacking of **Q'$_2$GaOC$_6$H$_4$CN** and **Q'$_2$GaOC$_6$H$_4$NO$_2$** compounds, that can be considered isostructural, are illustrated in **Figure 5.9**.

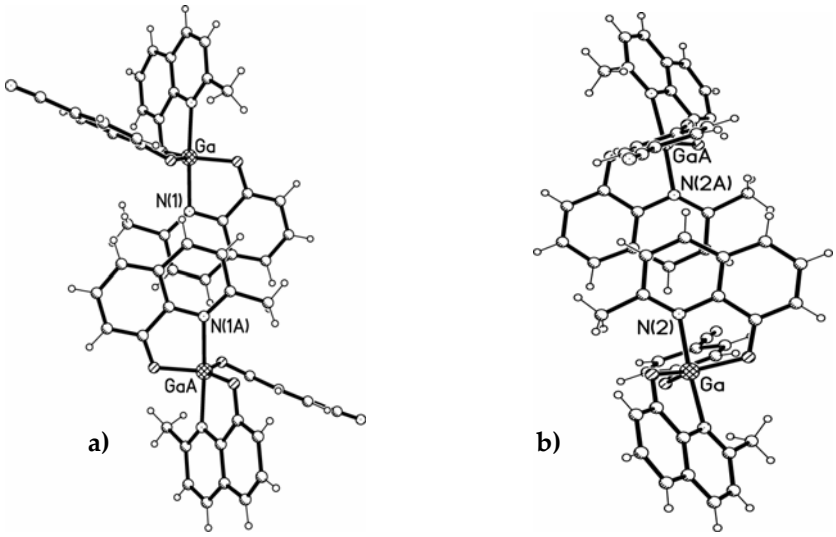

Figure 5.9: *orthogonal view of chelates stacking in* ***Q'$_2$GaOC$_6$H$_4$CN*** *or* ***Q'$_2$GaOC$_6$H$_4$NO$_2$***

The different offset in the OFF interactions between the Q'$_B$ chelates observed in complexes **Q'$_2$GaOC$_6$H$_4$CN** and **Q'$_2$GaOC$_6$H$_4$NO$_2$** is such that each chelate shows two contacts: a pyridyl–pyridyl [N(2)–C(19)] interaction, above the mean plane of the Q'$_B$ ligand, and a phenolate–phenolate [C(11)–C(16)] stacking below it, with the generation of chains running approximately along the *b* axis as shown in **Figure 5.9**, drawing **b** and in **Figure 5.10**, drawing **c**, illustrating the crystal packing of complex **Q'$_2$GaOC$_6$H$_4$CN** view down the *a* axis showing the

Q'$_B$ stacking contacts; while in the drawing (**d**) is showed the generation of chains running along the *b* axis .

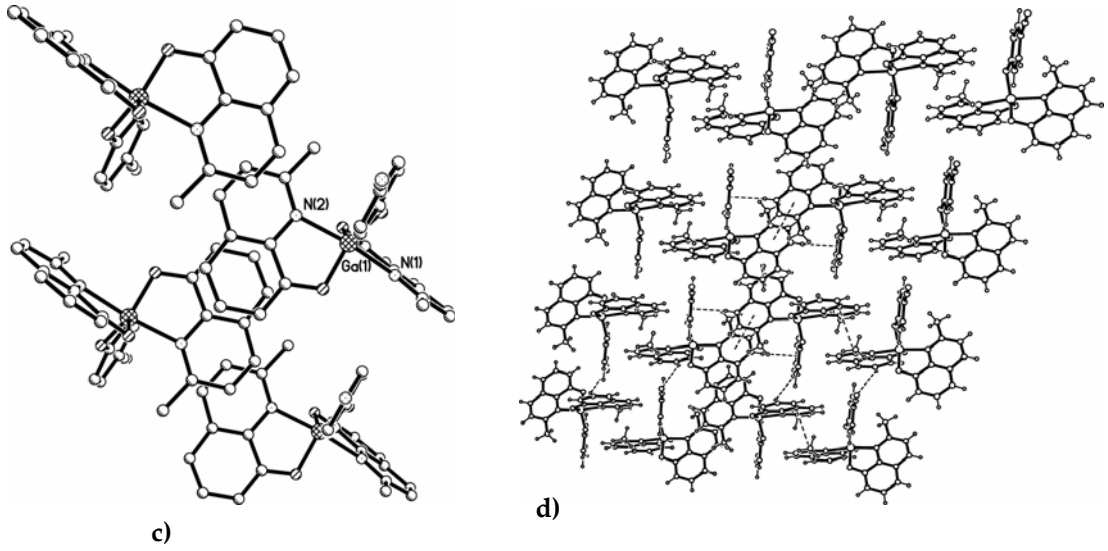

Figure 5.10: *crystal packing of complex* ***Q'$_2$GaOC$_6$H$_4$CN****.*

In both cases the presence of edge-to-face interactions involving the **OC$_6$H$_4$CN** and **OC$_6$H$_4$NO$_2$** rings, respectively, gives rise to a combination of three OFF and two EF interactions as a supramolecular secondary motif, connecting three molecules together, **Figure 5.10**, drawing **d**.

These repetition units are linked between π–π interactions involving the Q'$_A$ chelates of symmetrical molecules.

As a final confirmation of the lack of any polymorphism in the Ga(III) derivatives **Q'$_2$GaOC$_6$H$_5$**, **Q'$_2$GaOC$_6$H$_4$CN** and **Q'$_2$GaOC$_6$H$_4$NO$_2$**, X-ray powder diffraction analysis on the bulk sample showed it to be identical in all cases to the single crystal used for structure determination.

5.2 Pentacoordinated bimetallic complexes

The phenoxyde shows high reactivity towards gallium(III) as observed with the stable monometallic pentacoordinated compounds so the gallium coordination chemistry was studied related to the formation of bimetallic pentacoordinated compounds, in order to understand the chemical behaviour of gallium(III) metal in aqueous solutions with the contemporary presence of the strong chelating agent 2-methyl-8-hydroxyquinoline and bisphenols ligands.

Bidentate phenols ligands (HL^n), illustrated in **Figure 5.11**, were chosen taking in account their chemical structure.

HL^4 **$HOC_6H_4(CH_2)_3C_6H_4OH$**

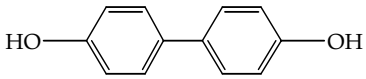

4,4'-biphenol

HL^5 **$HOC_6H_4C(CH_3)_2C_6H_4C(CH_3)_2C_6H_4OH$**

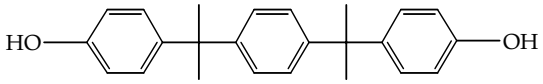

4,4'-(1,4-pheylenediisopropylidene)bis-phenol

HL^6 **$HOC_6H_4(CH_2)_3C_6H_4OH$**

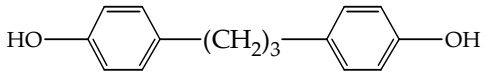

2,2'-bis-(4-hydroxyphenyl)-propane

Figure 5.11: *bidentate phenol ligands (HL^n).*

Thus, each ligand bear some structural characteristic:

- 4,4'-biphenol **$HOC_6H_4C_6H_4OH$** (**HL^4**)**,** with two aromatics rings directly covalently linked,
- 4,4'-(1,4-phenylenediisopropylidene)bis-phenol, **$HOC_6H_4C(CH_3)_2C_6H_4C(CH_3)_2C_6H_4OH$**, (**$HL^5$**), in which the aromatics rings are spaced by methyl groups.

- 2,2′-bis-(4-hydroxyphenyl)-propane **$HOC_6H_4(CH_2)_3C_6H_4OH$**, (**HL^6**) with the three methylene groups is an example of flexible ligand.

The synthesis of all compounds was performed as previously described for the monometallic compounds but with HQ′:Ga:HL^n in 4:2:1 molar ratio (**Scheme 5.2**). The ligands were activated with sodium hydroxide in ethanol solution then slowly added to an aqueous solution of gallium(III) nitrate hydrate. Some minutes after the ethanolic solution of 2-methyl-8-hydroxyquinoline was slowly added to the reaction mixture that was refluxed for six hours and under stirring overnight.

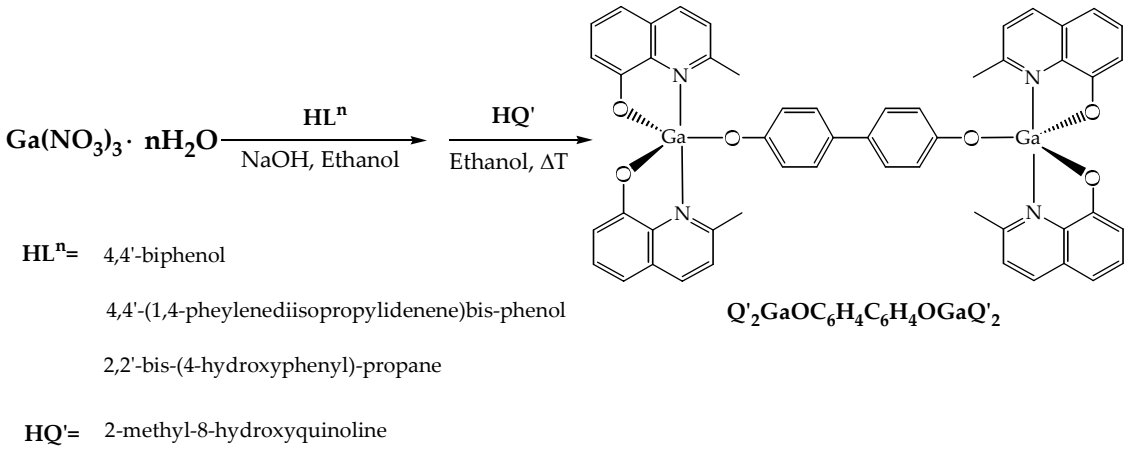

***Scheme 5.2**: synthetic procedure of bimetallic gallium complexes.*

The product were collected and washed with water ethanol and diethyl ether, to obtain solids at list 40% of reaction yields, which colour ranging from yellow to light green. But, because of the competitive formation of GaQ'_3, which presence was checked by ^{1}H NMR analysis, only **$Q'_2GaOC_6H_4C_6H_4OGaQ'_2$** compound was obtained with high purity confirmed by elemental analysis.

The melting point wasn't observed at temperature below 350°C. IR spectra show the methyl stretching around 3065 cm^{-1} and the typical bands of the chelated 2-methyl-8-hydroxyquinoline in the range 1605 – 1100 cm^{-1}. ^{1}H NMR data were collected in *d_6*-DMSO. The quinaldinate moieties are magnetically

equivalent nd the $H^{b,b'}$ are shifted to high frequency respect to those of **Q'$_2$GaOC$_6$H$_5$**.

5.3 Multimetallic Gallium (III) complexes

Pentacoordinated bimetallic gallium(III) compounds, synthesised with the right phenol ligands, open the possibility to synthesis more complex chemical structures. The idea is to build a multimetallic compound bearing more than two *Q'$_2$Ga-* fragments. In order to exploit the chemical affinity between phenols with particular structural properties and gallium(III) [5,10,15,20-tetrakis(4-hydroxyphenyl)-21*H*,23*H*-porphyrin], **H$_2$TPP(OH)$_4$**, reported in **Figure 5.12**, has been selected to be tested in reactions for the synthesis of mixed metallic complexes.

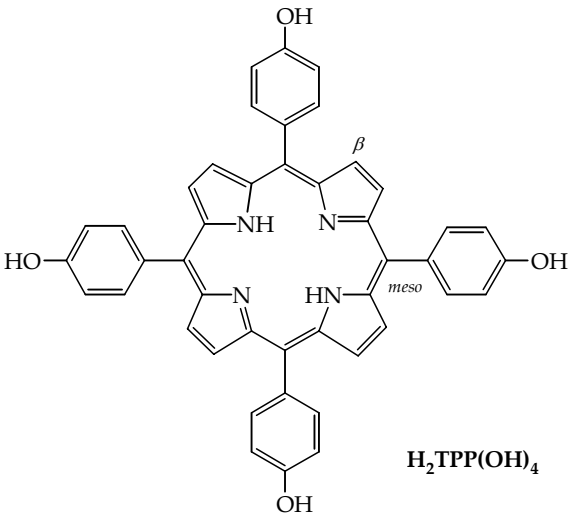

Figure 5.12: *5,10,15,20-tetrakis(4-hydroxyphenyl)-21H,23H-porphyrin* ***H$_2$TPP(OH)$_4$***

Porphyrin are rigid heteroaromatic macrocycles with an extended insaturation. These molecules are interesting because of the versatility of their chemical structure. Indeed, by introducing different chemical substituent on the β and/or

meso positions, it is possible to modulate both chemical and physical properties. Further the centre of the heteroaromatic ring can host a metal cation with the suitable ionic radius.[7-9]

Then **H_2TPP(OH)$_4$**, bearing in each *meso* position a phenol function and a metal cation in the central cavity, can be complexed as a rigid aromatic ligand acting a linker between more than two *Q′$_2$Ga-* fragments as illustrated in the **Scheme 5.3**.

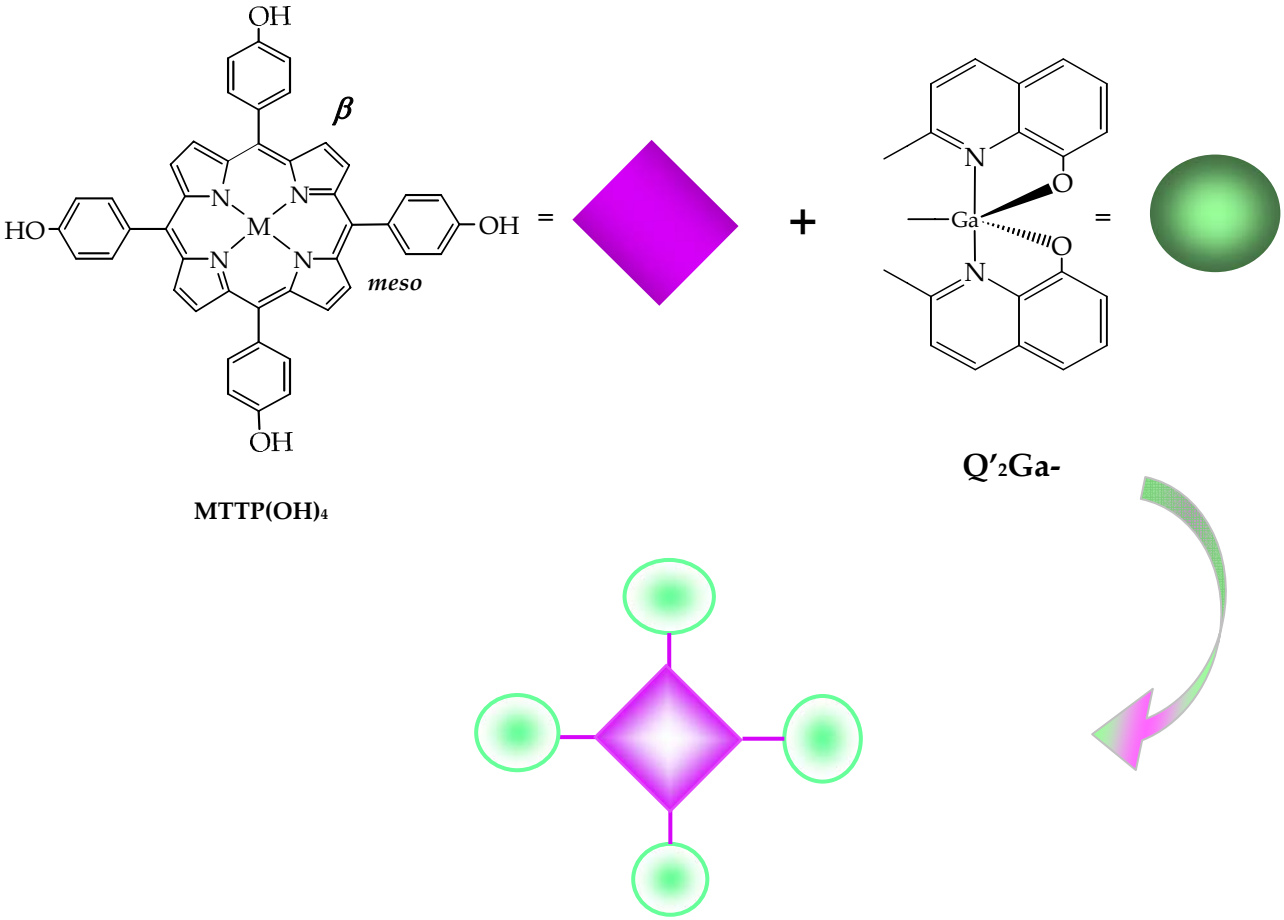

Scheme 5.3: *example of assemblated structure.*

The synthesis of the desired heterobimetallic structure was performed in two steps. The aromatic ring centre of **H_2TPP(OH)$_4$** was complexed with zinc acetate dehydrate in 1:1 molar ratio as reported in **Scheme 5.4**.

H_2TPP(OH)$_4$ was solved under energetic stirring in tetrahydrofurane at room temperature, then a methanolic solution of zinc acetate dihydrate was slowly

added. Suddenly, the reaction mixture colour has changed from light violet to dark violet. The reaction mixture was allowed to stir over night. The solvent of the reaction mixture was dried by evaporation under vacuum and the dark violet solid was collected and washed many time with water and with a small amount of diethyl ether.

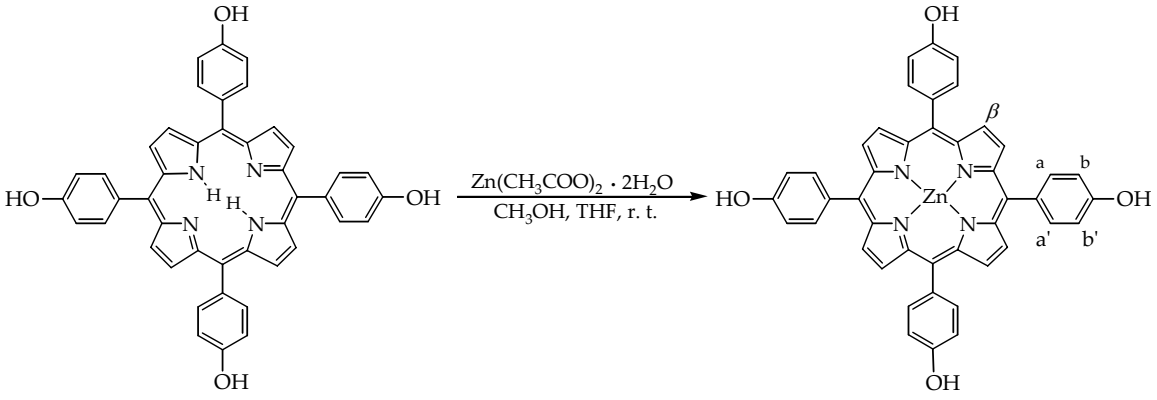

Scheme 5.4: *synthesis of ZnTPP(OH)₄· 2H₂O.*

The product, **ZnTPP(OH)₄**, was obtained in very good yields at list 70 %. It shows very high solubility in diethyl ether and in alcohols but is insoluble in chloroform, further it shows a weak hygroscopicity, so the compound was dried at 100°. The melting point wasn't observed at temperature below 350°C. Elemental analysis confirm the purity of the compound. IR spectra show the broad band of the phenol chemical functions at 3306 cm^{-1} and the CH stretching of the aromatic ring around 2920 cm^{-1}. Narrow and intense bands were observed in the range between 1607 – 998 cm^{-1}. ^{1}H NMR spectra were collected in methanol. As can be observed all protons are magnetically equivalent so the profile spectra shows one signal for each kind of proton. The four β protons are deshield at 8.86 ppm because of the extended conjugation of the aromatic rings. The phenol signals of $H^{a,a'}$ and $H^{b,b'}$ are found at 8.00 ppm and 7.18 ppm respectively, slightly shifted to higher frequency respect to zinc free porphyrin.

The synthetic second step, to obtain the desired polymetallic compound, was performed following the procedure described for the monometallic gallium compounds previously illustrated.

ZnTPP(OH)$_4$ was activated with NaOH, 1:4 molar ratio, then this suspension was slowly added to an aqueous solution of gallium(III) nitrate hydrate. Successively an ethanolic solution of 2-methyl-8-hydroxyquinoline was slowly added to the reaction mixture to obtain **ZnTPP(OH)$_4$**:Ga:HQ′ in 1:4.5:8 molar ratio as illustrated in the **Scheme 5.5**. After a six hours reflux and overnight stirring, a greenish blue solid was filtered.

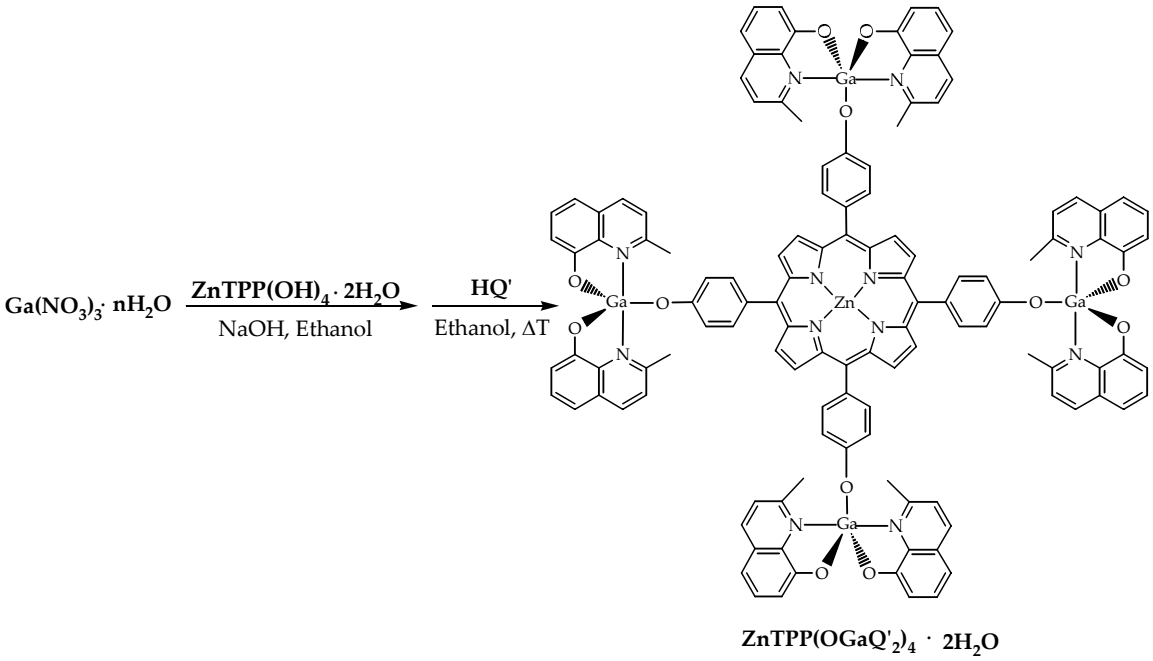

Scheme 5.5: *synthesis of ZnTPP(OGaQ′$_2$)$_4$.*

The collected powder was washed with water, ethanol, and small amounts of diethyl ether and chloroform to obtain a blue solid in 70% of reaction yield. Melting point wasn't observed at temperature below 350°C. The purity and the structure of **ZnTPP(OGaQ′$_2$)$_4$** were confirmed by elemental analysis and by spectroscopy. IR spectra show the methyl groups stretching at 3051 cm^{-1} the

typical band of the phenol hydroxyl group is disappeared. The presence of the chelated 2-methyl-8-hydroxyquinoline is revealed in the range between 1601 cm^{-1} and 1114 cm^{-1}. ^1H NMR spectra were registered in deuterated methanol and the presence of the Q'_2Ga- fragment is showed by one set of signals as well as the porphyrin moiety.

In order to study the reactivity of this kind of chemical systems, where one or more quinaldinate gallium fragment can be introduced on the periphery of the porphyrin moiety, other synthesis were performed with different **ZnTPP(OH)$_4$**:Ga:HQ′ molar ratio as shown in the **Scheme 5.6**.

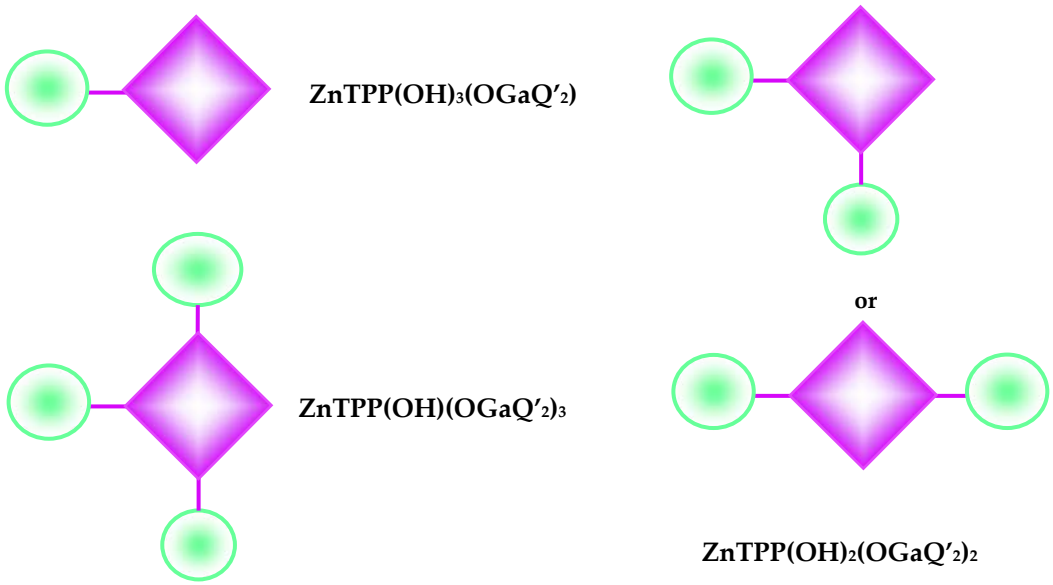

Scheme 5.6: *possible assembled structures.*

The synthesis of **ZnTPP(OH)$_3$(OGaQ'$_2$)**, **ZnTPP(OH)$_2$(OGaQ'$_2$)$_2$**, or **ZnTPP(OH)(OGaQ'$_2$)$_3$** compounds were obtained following the same procedure illustrated previously with **ZnTPP(OH)$_4$**:Ga:HQ′ respectively in 1:1:2, 1:2:4 and 1:2:6 molar ratio. IR and ^1H NMR analysis of all compounds were in agreement with the proposed structure as shown in **Figure 5.14**, but wasn't possible to distinguish if the resulting spectra were due to a single compound or to the contribution of a mixture of polymetallic species.[10]

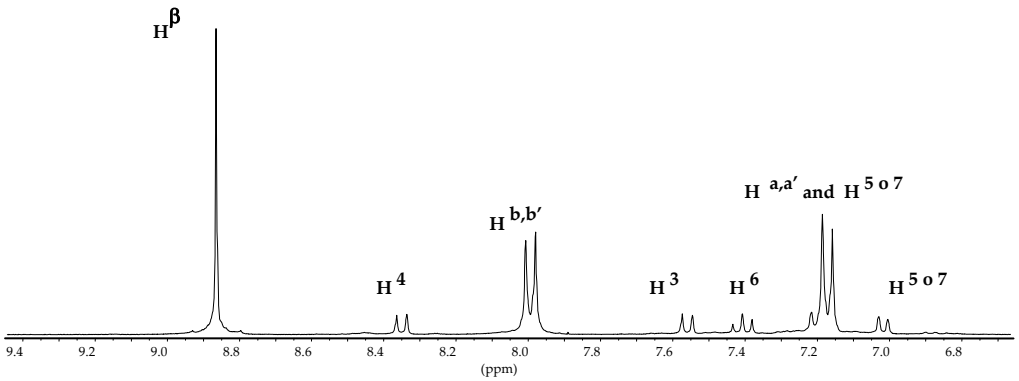

Figure 5.13: *typical ^{1}H NMR profile of the polymetallic species.*

The calculated values of the elemental analysis do not differentiate significantly the **ZnTPP(OH)$_3$(OGaQ'$_2$)**, **ZnTPP(OH)$_2$(OGaQ'$_2$)$_2$**, **ZnTPP(OH)(OGaQ'$_2$)$_3$**, **ZnTPP(OGaQ'$_2$)$_4$** species since the related C%, H% and N% values span the ranges 64.27 − 66.10, 4.26 − 3.72 and 7.25 − 7.22 respectively. While the elemental analysis give experimental values which do not perfectly agree for a unique pure species. Because of the difficulty to study the real structures and the purity degree of these products, as previously mentioned, MALDI/TOFMS (matrix assisted laser desorption/ionization tandem time-of-flight mass spectrometry) analysis were carried out.

The TOF spectrum of species **ZnTPP(OGaQ'$_2$)$_4$** is compatible with that of a mixture of compounds. In fact, it shows, besides the base peak at *m*/*z* 385, the species at *m*/*z* 740 that corresponds to the unreacted porphyrin (**ZnTPP(OH)$_4$**) and minor peaks at *m*/*z* 1124, 1508, 1892 and 2276 corresponding to ionized **ZnTPP(OH)$_3$(OGaQ'$_2$)**, **ZnTPP(OH)$_2$(OGaQ'$_2$)$_2$**, **ZnTPP(OH)(OGaQ'$_2$)$_3$**, and **ZnTPP(OGaQ'$_2$)$_4$**, respectively. All these species behave similarly when allowed to dissociate spontaneously, as shown by the corresponding MS/MS spectra. The ions at *m*/*z* 1892 and elemental composition [**ZnTPP(OH)(OGaQ'$_2$)$_3$**] afford, in fact, the species [ZnTPP(OGaQ'$_2$)$_2$ - H]$^+$ at *m*/*z* 1507, as shown in the expandex view of **Figure 5.14**, by homolysis of the O–Ga bond.

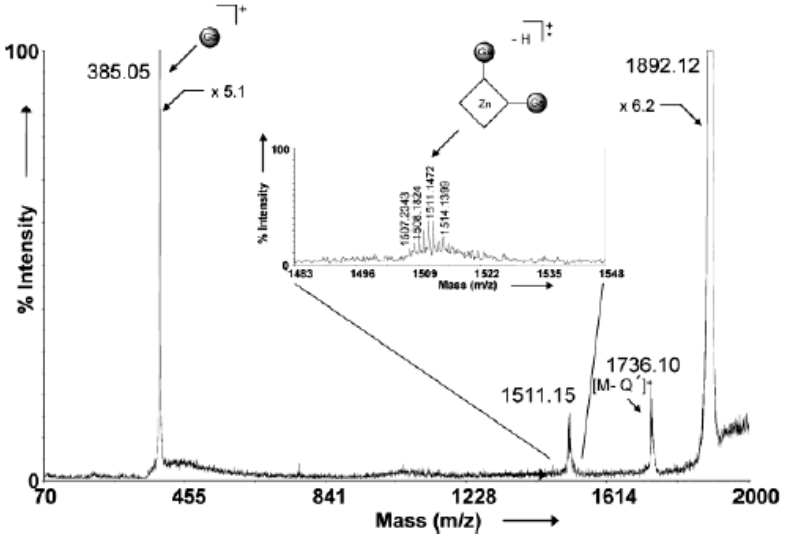

Figure 5.14: *TOF/TOF spectrum of the m/z 1892-1902 cluster.*

In order to study these compounds, 2,7-Dimeythoxynaphtalene (DMN) was tested and proposed[11] as new matrix to analyse low molecular weight complexes extremely labile species because of in the present study DMN has revealed the opportunity to use a softer methodology for this labile compounds sensible to the acidity of other typology of matrix.

With the experimental conditions described previously the main product is Ga_4/Zn is very hard to purify properly so that, traces of the homologous polymetallic species (Ga_3/Zn, Ga_2/Zn or Ga/Zn) which usually form together with Ga_4/Zn, cannot be effectively removed. Although the MALDI/TOFMS[11] data do not allow a quantitative estimation of the relative abundance of the different polymetallic complexes, on the bases of both the reproducibility of the preparation and the values of the data were obtained, the **ZnTPP(OH)(OGaQ'$_2$)$_3$**, **ZnTPP(OH)$_2$(OGaQ'$_2$)$_2$** and **ZnTPP(OH)$_3$(OGaQ'$_2$)** species are present in traces only, and that these traces do not affect the results of the spectroscopic measurements.

5.3.1 Multimetallic gallium complexes: different synthetic pathway

A different synthetic pathway was explored in order to overcome the problematic results previously described. Because of the difficulties come from the incomplete complexation of the phenol chemical function in the peripheral porphyrin sites, the strategy was follow the inverse synthetic route, first, introducing the *Q'₂Ga*– fragment then the zinc insertion in the porphyrinic core, adapting the usual synthesis, as illustrated in **Scheme 5.7**.

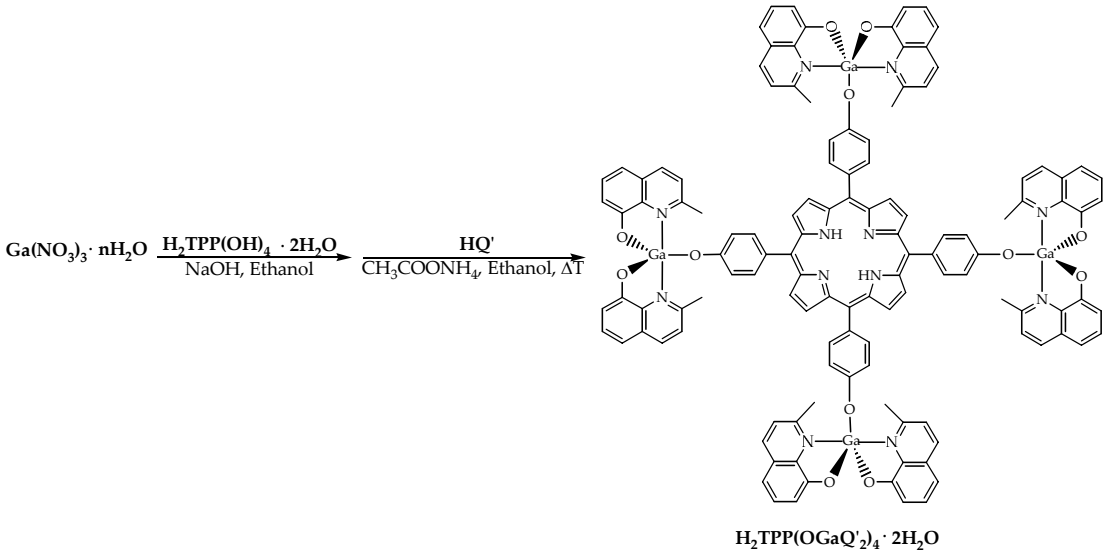

Scheme 5.7: *synthesis of H₂TPP(OGaQ'₂)₄.*

The obtained product is a dark purple, insoluble solid in 42% reaction yield. Melting point wasn't observed a temperature below 350°C. The elemental analysis confirm the purity of this compound and infrared spectra are consistent with the presence of quinolinate fragments, but because of the poor solubility of **H₂TPP(OGaQ'₂)₄**, ^{1}H NMR spectra wasn't registered.

The solid was suspended in ethanol and a slightly excess of zinc acetate dihydrate was added (**Scheme 5.8**).

$$\mathbf{H_2TPP(OGaQ'_2)_4 \cdot H_2O} \xrightarrow[\text{Ethanol, } \Delta T]{\mathbf{(CH_3COO)_2Zn \cdot 2H_2O}} \mathbf{ZnTPP(OGaQ'_2)_4 \cdot H_2O}$$

Scheme 5.8: *reaction with zinc acetate.*

A dark violet solid was obtained with a 50% of reaction yield. As expected, the melting point wasn't observed, the infrared spectra are consistent with the presence on a chelated 2-methyl-8-hydroxyquinoline and an intense band stretching at 997 cm^{-1} could be associated to the metalation of the porphyrinic core. Also in that case ^1H NMR analyses were not allowed because of the poor solubility. The last synthetic test was to introduce in the porphyrinic core a gallium atom to obtain an homopolymetallic compound the synthesis was carried out with **$H_2TPP(OH)_4$**:Ga:HQ' in 1:5:8 molar ratio. After sixteen hours under reflux, a small amount of litium chloride was added to induce metathesis on the axial position of the gallium in the porphyrinic core, as shown in the **Scheme 5.9,** the reaction mixture was allowed to stir for 24 hours under ambient temperature.

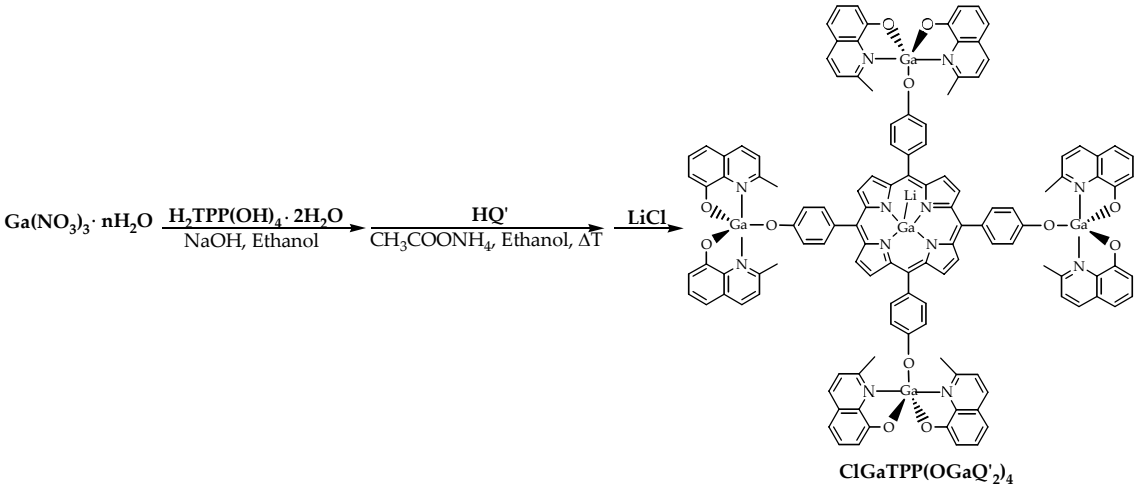

Scheme 5.9**: synthesis of **ClGaTPP(OGaQ'$_2$)$_4$.

A dark bluish violet powder was isolated with a good reaction yield. The elemental analysis are consistent with the compound purity. Unlikely the solid is insoluble, so ^1H NMR wasn't registered.

5.4 Gallium(III) pentacoordinated complexes with carboxylic acids

Gallium(III) pentacoordinated compounds obtained with HQ':Ga in 2:1 molar ratio, and a third monodentate ligand (HL'^{n}) chosen among mono and bidentate carboxylic acid, *p*-substituted benzoic acids derivatives, or halides, are known in literature. These compounds were studied for long of time only from the structural point of view to understand the gallium chemistry and the selective chelating properties of 2-methyl-8-hydroxyquinoline and the high affinity of gallium(III) towards carboxylate. This class of pentacoordinate compounds has revealed interesting structural and chemical features. To improve these properties a series of new pentacoordinated gallium(III) complexes were synthesised choosing substituted benzoic acids and bidentate carboxylic acids.

5.4.1 monometallic gallium compounds with benzoic derivatives

The synthesis were performed adapting the synthetic protocol previously described. To achieve pentacoordination in the bischelated *Q'*$_2$*Ga*– fragment, *p*-nitrobenzoic acid, *p*-hexyloxybenzoic acid and *p*-octyloxybenzoic, showed in **Figure 5.15**, were chosen as monodentate ligand HL'^{n}.

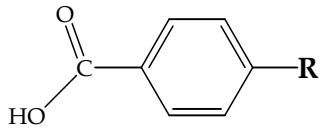

HL'^{1}	**R=**	$-NO_2$
HL'^{2}		$-O(CH_2)_5CH_3$
HL'^{3}		$-O(CH_2)_7CH_3$

Figure 5.15: *p-substituted benzoic ligands (HL'^{n}).*

Scheme 5.10 report the reaction procedure to obtain the desired compounds **Q′$_2$GaOOCC$_6$H$_4$NO$_2$** and **Q′$_2$GaOOCC$_6$H$_4$O(CH$_2$)$_5$CH$_3$**.

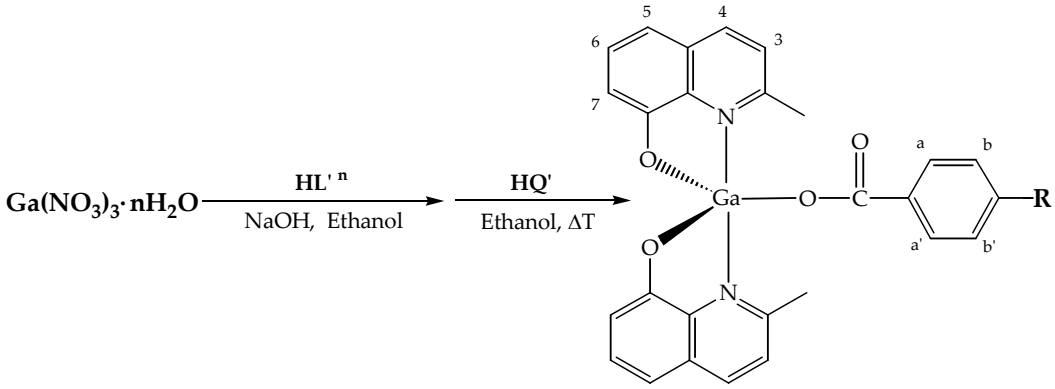

Scheme 5.10: *synthetic procedure of Q′$_2$GaL′^{n} p-substituted benzoic acid.*

All compounds were obtained as green microcrystalline powder with at list 50% of reaction yields. The purity and the structures were confirmed by elemental analysis and spectroscopic characterization.

The melting point of **Q′$_2$GaOOCC$_6$H$_4$NO$_2$** compound was 267 – 270°C while those of **Q′$_2$GaOOCC$_6$H$_4$O(CH$_2$)$_5$CH$_3$** was 203 - 205°C. The lowered melting point of this last compound, respect to those typically showed by bisquinaldinate compounds, is probably due to the presence of the aliphatic chain. The structure is confirmed by the presence in the infrared spectra of the C–H stretching bands of the *–CH$_3$* group at 3051 cm^{-1} for the *p*-nitrobenzoic derivative, and at 3065 cm^{-1} for *p*-hexyloxybenzoic derivative, further for this last compounds intense bands in the 2951-2870 cm^{-1} range are attributed to the C–H stretching of the aliphatic chain. The presence of the C=O group is revealed in an intense stretching band at 1660 cm^{-1} in the spectra of **Q′$_2$GaOOCC$_6$H$_4$NO$_2$**.

This band is shifted at 1650 cm^{-1} in **Q′$_2$GaOOCC$_6$H$_4$O(CH$_2$)$_5$CH$_3$** compound. The bands in the range between 1606 cm^{-1} and 1114 cm^{-1} represent the chelated quinolinate fragment in both compounds. The bisquinolinate fragment shows only one set of signals in the ^{1}H NMR spectra registered in $CDCl_3$. The $H^{a,a'}$ of *p*-nitro benzoic derivative is shifted about 1.40 ppm to high frequency respect to those of **Q′$_2$GaOOCC$_6$H$_4$O(CH$_2$)$_5$CH$_3$** compound**,** while $H^{b,b'}$ is slightly shifted to high frequency. The presence of the aliphatic chain in of the *p*-hexyloxy derivative compound is revealed by a sequence of signals at low frequencies.

A different pathway was exploit to obtain pentacoordinated compounds.

So starting from the phenolate derivative complex **Q′$_2$GaOC$_6$H$_5$**, the phenolate ligand was substituted by the *p*-octyloxybenzoate to obtain **Q′$_2$GaOOCC$_6$H$_4$O(CH$_2$)$_7$CH$_3$** complex as showed in the reaction **Scheme 5.11**.

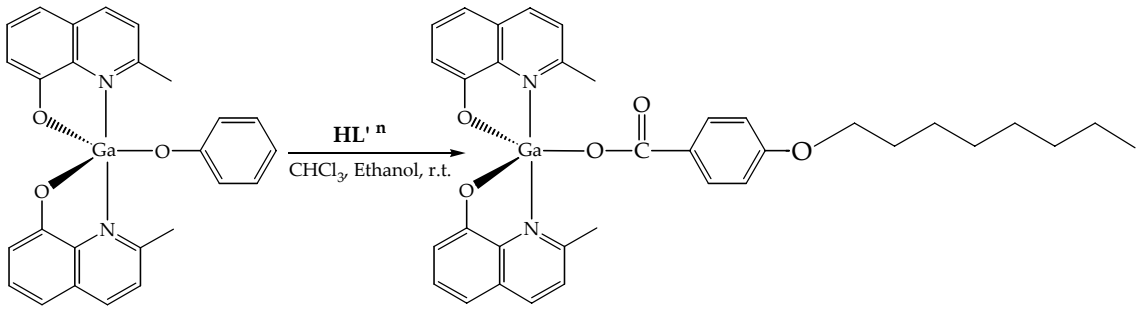

Scheme 5.11*: different synthetic procedure of Q′$_2$GaL′$_n$ obtained with p-octyloxybenzoic acid.*

The *p*-octyloxybenzoic ligand was activated with sodium hydroxide in ethanol and slowly added to a chloroform solution of **Q′$_2$GaOC$_6$H$_5$**, in 10:1 molar ratio, to obtain a green microcrystalline solid in 30% reaction yield.

The ligand substitution was confirmed by elemental analysis and by spectroscopy, as expected the melting point was lowered towards 185–187°C. The infrared spectra confirm the compound structure, with the stretching band

of the methyl group at 3057 cm^{-1} and presence of the aliphatic chain is evidenced by C–H stretching bands in the range 2924 – 2854 cm^{-1}.

The C=O stretching is found at 1642 cm^{-1}. The typical quinolinate bands profile ranging from 1605 cm^{-1} to 1115 cm^{-1}.

^1H NMR spectra shows only one set of signals related to the magnetically equivalent quinolinate moieties. The chemical shift of the $H^{a,a'}$ and $H^{b,b'}$ protons are slightly shifted respectively to lower an higher frequencies respect to those of the free ligand. The aliphatic signals, found to low frequency, doesn't show any change in the chemical shift respect to the unlinked ligand.

The high affinity between gallium and carboxylates is demonstrated with the previous substitution reaction. Further, always microcrystalline solids were obtained directly from the reaction mixture.

5.4.2 Chemical structure of $\mathbf{Q'_2GaOOCC_6H_4O(CH_2)_5CH_3}$

The $\mathbf{Q'_2GaOOCC_6H_4O(CH_2)_5CH_3}$ complexes was structurally characterized by X-ray diffraction analysis on single crystal. Good crystals were obtained from chloroform/*n*-hexane mixture. The complex, which structure is shown in **Figure 5.17**, crystallize in the monocline $P2_1/c$ space group with two molecules in the asymmetric unit.

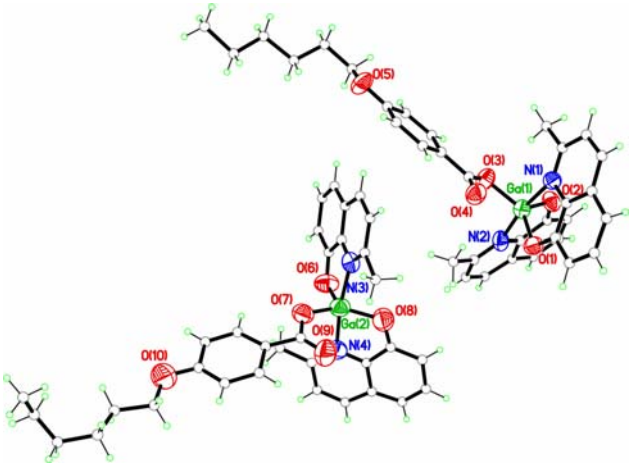

Figure 5.16: *cristalline structure of* $\mathbf{Q'_2GaOOCC_6H_4O(CH_2)_5CH_3}$ *complex.*

The coordination geometry around gallium atom is distorted trigonal bipyramid. The 2-methyl-8-hydroxyquinolinate moieties are coordinated to gallium through oxygen and nitrogen atoms. So the coordination sphere is completed by one molecule of carboxylate through an oxygen atom.

In the **Table 5.4**, the selected bond length and angles related to the coordination sphere are reported.

Ga(1)-O(1)	1.854(5)	Ga(2)-O(6)	1.835(6)
Ga(1)-O(2)	1.862(5)	Ga(2)-O(7)	1.839(6)
Ga(1)-O(3)	1.890(5)	Ga(2)-O(8)	1.853(7)
Ga(1)-N(1)	2.048(6)	Ga(2)-N(3)	2.033(7)
Ga(1)-N(2)	2.059(7)	Ga(2)-N(4)	2.069(7)
O(1)-Ga(1)-O(2)	115.2(2)	O(6)-Ga(2)-O(7)	105.6(3)
O(1)-Ga(1)-O(3)	135.3(2)	O(6)-Ga(2)-O(8)	121.3(3)
O(1)-Ga(1)-O(3)	109.4(3)	O(7)-Ga(2)-O(8)	133.1(3)
O(1)-Ga(1)-N(1)	84.8(2)	O(6)-Ga(2)-N(3)	83.0(3)
O(2)-Ga(1)-N(1)	90.7(2)	O(7)-Ga(2)-N(3)	94.6(3)
O(3)-Ga(1)-N(1)	97.9(2)	O(8)-Ga(2)-N(3)	89.9(3)
O(1)-Ga(1)-N(2)	90.8(2)	O(6)-Ga(2)-N(4)	92.8(3)
O(2)-Ga(1)-N(2)	82.(2)	O(7)-Ga(2)-N(4)	96.4(3)
O(3)-Ga(1)-N(2)	91.6(2)	O(8)-Ga(2)-N(4)	83.4(3)
N(1)-Ga(1)-N(2)	169.9(2)	N(3)-Ga(2)-N(4)	168.9(3)
Ga(1)-------O(4)	2.692(3)	Ga(2)-------O(9)	2.296(4)

Table 5.4: *bond lenght (Å) and angles (°) of* ***Q'$_2$GaOOCC$_6$H$_4$O(CH$_2$)$_5$CH$_3$.***

As it is possible to observe, the geometry is greatly distorted by the presence of the chelating ligands, so the two nitrogen atom in apical position (N(1) and N(2) in the molecule **1**; N(3) and N(4) in molecule **2**) deviate strongly from linearity because of the N–Ga–N angle is 169.2(2) and 168.9(3)°, respectively, in the two

molecules. The bite angles related to the chelated five terms rings, $\overline{\text{GaNOCC}}$, are 84.8(2) in the molecule **1**, and 83.0(3) in the molecule **2**; are similar to those observed in analogous gallium complexes.[2] The two chelated five terms rings $\overline{\text{GaNOCC}}$ in each molecules, are almost perpendicular each other, with dihedral angles between the middle plain of 68° (molecule **1**) and 59°(molecule **2**). The crystal packing is characterized by two typology of intermolecular interactions: hydrogen bond and π–π stacking interactions.

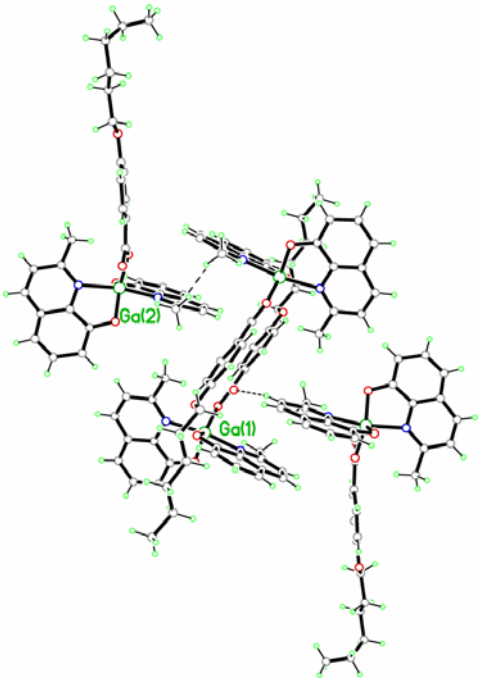

Figure 5.17: *crystal packing of* ***Q'$_2$GaOOCC$_6$H$_4$O(CH$_2$)$_5$CH$_3$*** *compound.*

Indeed, as evidenced in **Figure 5.17**, molecule **1** present weak hydrogen bond type interactions between oxygen atom O(4) of the carboxylate ligand not involved in the coordination and an hydrogen atom of the quinolinate pyridinic moiety of a molecule symmetrically correlated to the molecule **2** (O(4)---H(51a) = 2.47 Å, O(4)---C(51a) = 3.34 Å, C(51a)-H(51a)---O(4) = 156.7°, a = 3-*x*, 1-*y*, 1-*z*). The second type of intermolecular interaction consists of π–π stacking interactions between two quinolinate pyridinic ring belonging to molecule **2** and to a symmetrically correlated to the molecule **1**.

The interaction nature is evidenced by the interplanar distance similar to 3.61 Å (centroid distance of 4.18 Å), by the inclination angle of 30° and a trasversal slip of 1.82 Å.

5.5 Gallium complexes trisubstituted benzoic acids derivatives

A new series of compounds were synthesised to study which possible changes can be introduced in the physical and chemical properties of the pentacoordinated bisquinaldinate gallium(III). Starting from the previous synthetic observations, the affinity between the carboxylic chemical function and gallium(III) metal cation could be better exploited to introduce more substituents enhancing the complexity of the chemical structure. In order to investigate this aspect, substituted benzoic acid bearing aliphatic tales **$HOOCC_6H_2(OC_6H_{13})_3$**, HL'[4], and **$HOOCC_6H_2(OC_{14}H_{29})_3$**, HL'[5], as gallic acid derivative, as illustrated in **Figure 5.18**, were synthesised.

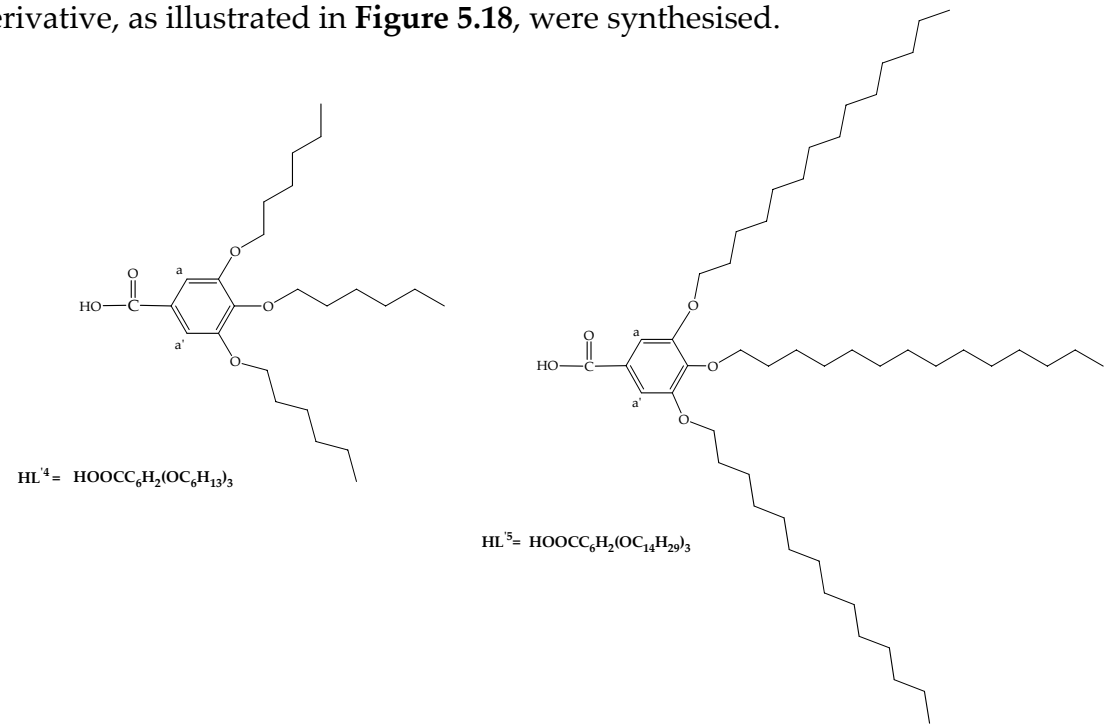

Figure 5.18: $HOOCC_6H_2(OC_6H_{13})_3$ and $HOOCC_6H_2(OC_{14}H_{29})_3$, gallic acid derivatives.

5.5.1 Synthesis of $HOOCC_6H_2(OC_6H_{13})_3$ *and* $HOOCC_6H_2(OC_{14}H_{29})_3$

The synthesis were carried out as illustrated in the **Scheme 5.12**, adapting the synthetic procedure reported in literature.[12,13] The etherification of the methyl ester, methyl 3,4,5-trihydroxybenzoate $CH_3OOCC_6H_2(OH)_3$, was performed in cyclohexanone. Potassium carbonate was added to the suspension with methyl ester:K_2CO_3 in 1:5.1 molar ratio. An excess of the suitable 1-bromo-alcane (1:3.1 molar ratio) was dropped to the reaction mixture suddenly a catalytic amount of potassium iodide was added. The brown reaction mixture was refluxed for 72 hours. After collection of the salts by filtration, the cyclohexanone solution was dried many time as azeotrope with water by evaporation under reduced pressure. A white solid was obtained by crystallization from $CHCl_3$/methanol.

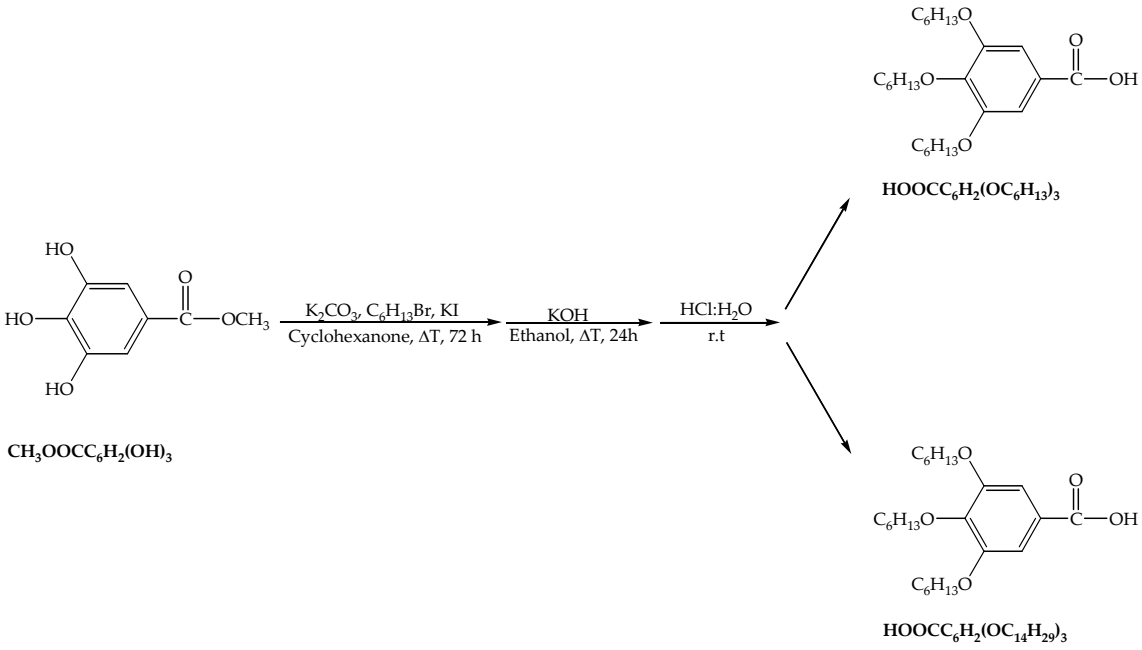

Scheme 5.12: *synthesis of* $HOOCC_6H_2(OC_6H_{13})_3$ *and* $HOOCC_6H_2(OC_{14}H_{29})_3$.

The obtained product was suspended under stirring in ethanol at 70°C then an aqueous solution of potassium hydroxide was added in order to obtain the

benzoic acid. After 24 hours under reflux the desired compound was precipitated by adding an acidic aqueous solution of HCl:H_2O in 2:10 volume ratio. The precipitated white product was washed with water and ethanol, then solved in warm petroleum ether and recrystallised at low temperature. The **$HOOC_6H_2(OC_6H_{13})_3$** compound was obtained as white solid in 70% of reaction yield. The compound purity and structure was confirmed by the usual characterization techniques. The melting point was found around 35-37 °C and the infrared spectra show the intense C–H stretching of the aliphatic chains in the range 2931 – 2638 cm^{-1} and the presence of the carbonyl group at 1687 cm^{-1}. ^1H NMR spectra, collected in $CDCl_3$, confirm the presence of the three aliphatic chains at low frequencies. The **$HOOC_6H_2(OC_{14}H_{29})_3$** compound was collected as white solid with a 60% of reaction yield and the elemental analysis confirm its purity. This compound show good solubility in chloroform and slightly in diethyl ether. IR spectra show two narrow and intense bands at 2919 cm^{-1} and 2849 cm^{-1} respectively. The carbonyl group stretching was found at 1682 cm^{-1}. ^1H NMR spectra reveal the presence of the three aliphatic chains without any change in the chemical shift respect to the compound **$HOOC_6H_2(OC_{14}H_{29})_3$**. DSC analysis reported in literature reveal liquid phase at 74°C and mesomorphysm interval 45°C –Tc.

5.5.2 Synthesis of $Q'_2GaOOCC_6H_2(OC_6H_{13})_3$ and $Q'_2GaOOCC_6H_2(OC_{14}H_{29})_3$

The synthesis of pentacoordinated gallium(III) compound **$Q'_2GaOOCC_6H_2(OC_6H_{13})_3$** and **$Q'_2GaOOCC_6H_2(OC_{14}H_{29})_3$** was performed adapting the method described for this class of compounds as reported in the **Scheme 5.13**, and taking in account the difficulties due to the solubility features of the benzoic monodentate ligands. The ligands **$HOOC_6H_2(OC_6H_{13})_3$** and **$HOOC_6H_2(OC_{14}H_{29})_3$** were suspended in ethanol with potassium hydroxide in

1:2 molar ratio, small amounts of diethyl ether were added to enhance the benzoic acids solubility, then the reaction mixture was allowed to stir for 24 hours at room temperature.

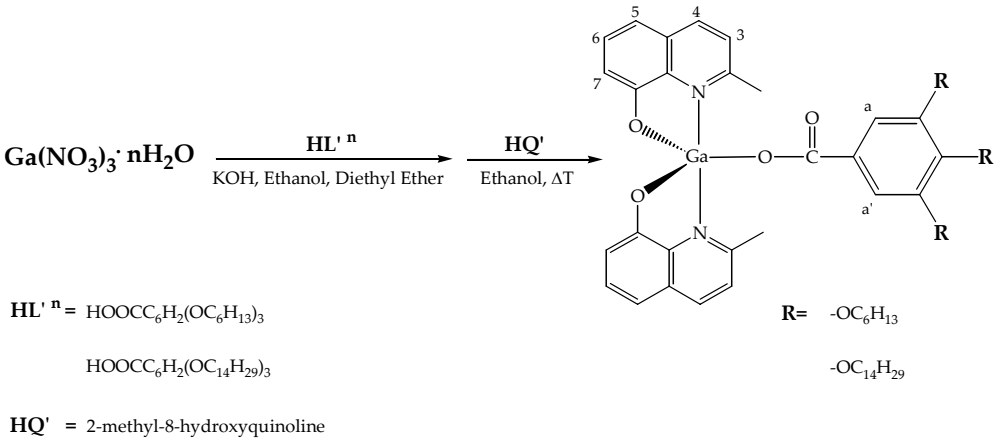

Scheme 5.13: *synthesis of* $Q'_2GaOOCC_6H_2(OC_6H_{13})_3$ *and* $Q'_2GaOOCC_6H_2(OC_{14}H_{29})_3$.

The activated ligands were slowly added to an ethanolic solution of gallium(III) nitrate hydrate under energetic stirring, after 15 minutes an ethanolic solution of 2-methyl-8-hydroxyquinoline was slowly added to the reaction mixture. That suspension was refluxed for six hours then was allowed to stir overnight.

The reaction mixture was dried by evaporation under vacuum to give a solid again dissolved in chloroform to be filtered on Celite powder. The obtained chloroform solution was dried by evaporation under vacuum. The green solid was dissolved in small amount of chloroform then a small quantity of methanol was added to induce crystallization at very low temperatures. A green microcrystalline precipitates was obtained. The green solid was washed with small amounts of very cold diethyl ether and acetone to obtain the desired compound. The ligands aren't soluble in ethanol, further the presence of three aliphatic chains influence the reactivity of these compounds. So the reaction yields were quite low. The purity of the obtained green microcrystalline solids was confirmed by elemental analysis. The infrared spectra of the two compounds show the typical bands profile of a pentacoordinated gallium(III)

bisquinaldinate complex. Indeed around 3064 cm^{-1} it is possible to observe the C–H stretching of the methyl group, and the intense C–H stretching bands of the aliphatic chains in the 2931–2859 cm^{-1} range for **Q′$_2$GaOOCC$_6$H$_2$(OC$_6$H$_{13}$)$_3$** compound and in the 2917–2851 cm^{-1} range for **Q′$_2$GaOOCC$_6$H$_2$(OC$_{14}$H$_{29}$)$_3$** compound. The stretching band of the carbonyl group was observed 1649 cm^{-1} shifted to higher frequencies respect to the *free* ligands. The presence of the chelated 2-methyl-8-hydroxyquinoline is revealed in the range between 1586–1115 cm^{-1}. As illustrated in **Figure 5.19**, the desired structure was confirmed by ^{1}H NMR spectra.

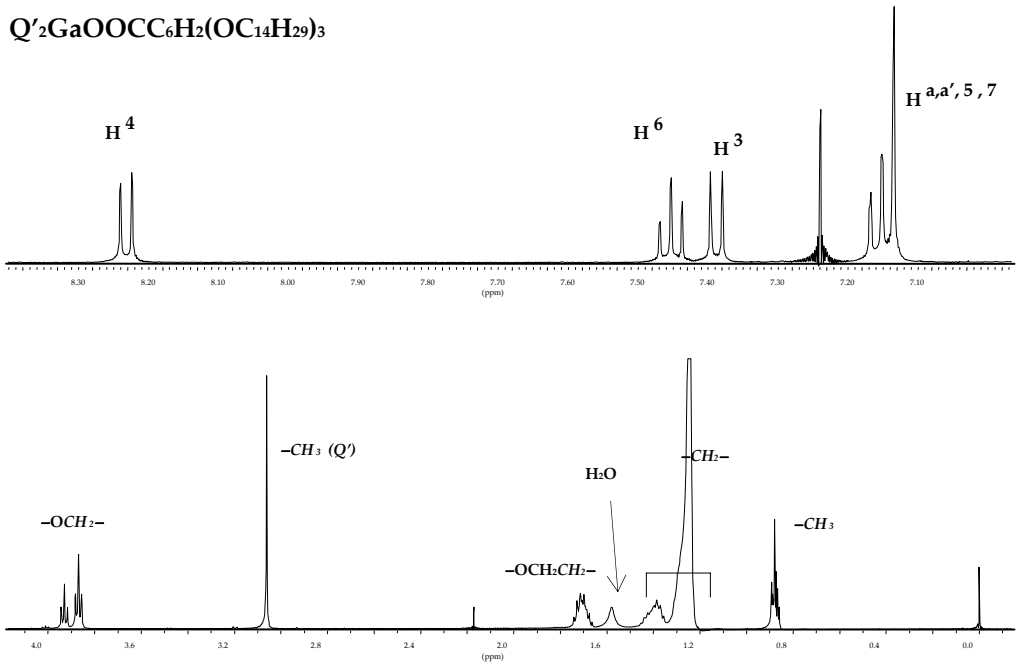

Figure 5.19: *^{1}H NMR spectra of* ***Q′$_2$GaOOCC$_6$H$_2$(OC$_{14}$H$_{29}$)$_3$***

The redox potentials measured versus ferrocene show the same behaviour explained previously with the gallium phenolate compounds. CV analyses showed no reduction waves for all complexes inside the solvent window. Oxidation processes are evident as irreversible waves above 1433 mV for **Q′$_2$GaOOCC$_6$H$_2$(OC$_6$H$_{13}$)$_3$** and 1440 mV for **Q′$_2$GaOOCC$_6$H$_2$(OC$_{14}$H$_{29}$)$_3$**. The non

well-defined irreversible oxidation waves and the precipitation at the Pt working electrode surface prevent further analysis.

Moreover, complex **Q'$_2$GaOOCC$_6$H$_2$(OC$_6$H$_{13}$)$_3$** has been characterized in the solid state by X-ray diffraction analysis on single crystal. Crystal packing and supramolecular motif are still under investigation.

As shown in **Figure 5.20**, the angles around the Ga(III) ion approximate a trigonal bipyramid geometry, with the two Q' ligands in an N,N *trans* conformation (N–Ga–N angle of 171.5(1)°).

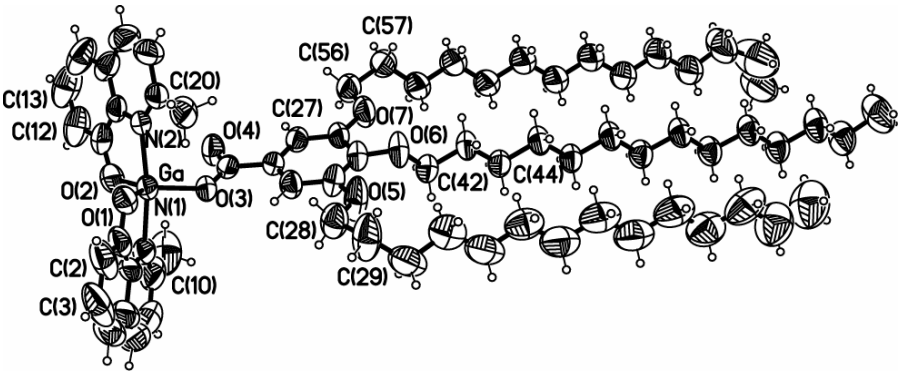

Figure 5.20: *Perspective view of* ***Q'$_2$GaOOCC$_6$H$_2$(OC$_6$H$_{13}$)$_3$*** *complexes with atomic numbering scheme (ellipsoids at the 50% level).*

All the geometrical parameters such as bond distances and angles are comparable with those values found in the other pentacoordinated Ga(III) complexes previously discussed. Only one of the three alkoxy chains shows a *trans* conformation, while the other two exhibit one and two gauche configurations of C–C bonds revealed also in ^{1}H NMR spectra by the two signals of –O*CH*$_2$– protons..

The melting point of **Q'$_2$GaOOCC$_6$H$_2$(OC$_6$H$_{13}$)$_3$** was observed at 160-164°C. While the presence of long aliphatic chains in the molecular structure of **Q'$_2$GaOOCC$_6$H$_2$(OC$_{14}$H$_{29}$)$_3$** suggest different thermal behaviour, in fact phase

transitions ware detected by DSC. The thermographs were collected at the heating and cooling rate of 10 °C/min. In the heating run two endothermic peaks at 68 °C and a 154 °C were detected while in the cooling run two exothermic peaks were observed at 46 °C and 144 °C. Further study on the phase transition characteristics are still under investigation.

5.6 Pentacoordinated complexes obtained with bifunctional carboxylic acids

A series of bimetallic compounds were synthesised exploiting the reactivity of carboxylate derivative in order to link two Q'_2Ga- fragments. The bifunctional carboxylic acid were chosen on the basis of the central unit characteristics. therephtalic acid **$HOOCC_6H_4COOH$**, acetilenic acid **HOOCC≡CCOOH** and dodecandicarboxylic acid **$HOOC(CH_2)_{12}COOH$** could be some examples of rigid aromatic or insature or flexible central unit. As illustrated in the **Scheme x**, the synthetic pathway was similar to those reported for the previous compounds also for **$Q'_2GaOOCC{\equiv}CCOOGaQ'_2$** complex reported in literature with a different synthetic procedure.[2]

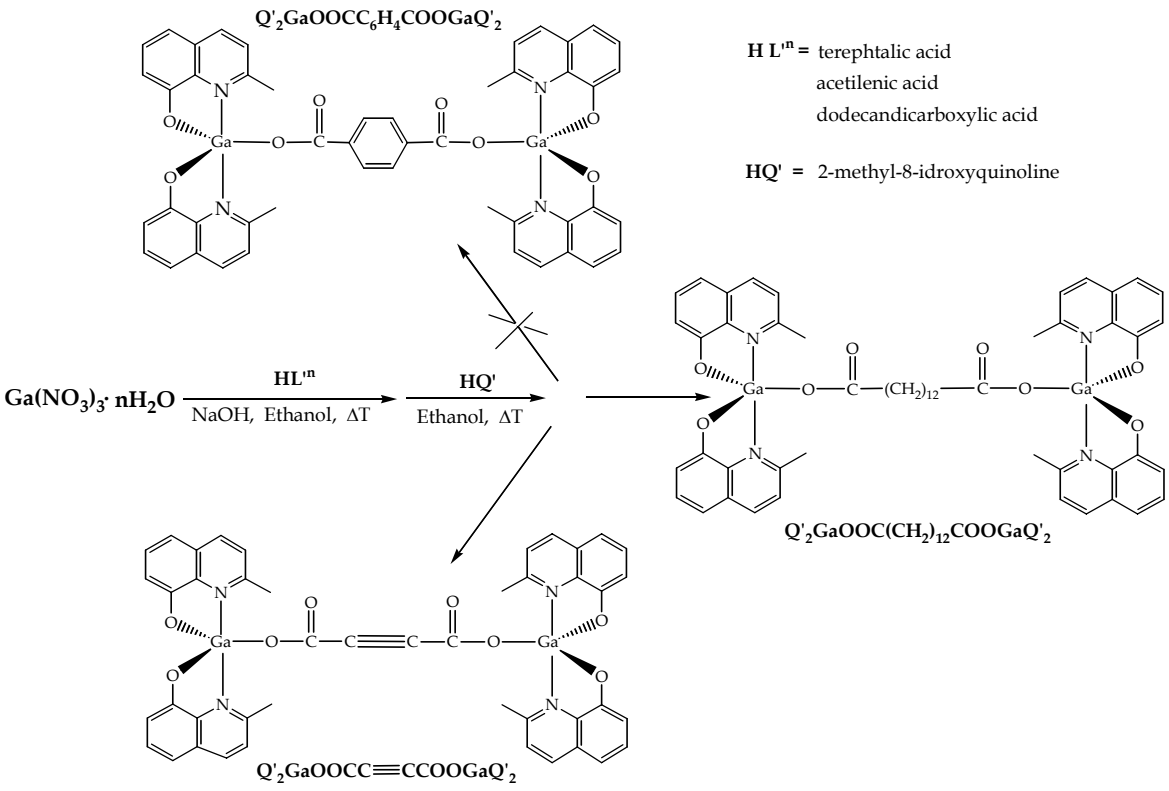

Scheme 5.14: *pentacoordinated bimetallic compounds.*

The **Q′₂GaOOCC≡CCOOGaQ′₂** and **Q′₂GaOOC(CH₂)₁₂COOGaQ′₂** compounds are light green solids recrystallized from chloroform/*n*-hexane mixture to obtain reaction yields ranging from 34% to 40%. Only the complex **Q′₂GaOOC(CH₂)₁₂COOGaQ′₂** shows low melting point around 172-174°C. The purity of all compounds was confirmed by elemental analysis except for **Q′₂GaOOCC₆H₄COOGaQ′₂** because of the presence of GaQ′₃ as impurity checked by ^{1}H NMR spectroscopy. In the infrared spectra of all compound the C–H stretching bands of the methyl group ranging from 3069 cm^{-1} to 3046 cm^{-1}. In the case of **Q′₂GaOOC(CH₂)₁₂COOGaQ′₂** complex, at 2925 cm^{-1} and 2852 cm^{-1} it is possible to observe the narrow and intense band stretching of the aliphatic C–H. The C=O stretching ranging from 1669 cm^{-1} to the very strong band at 1664 cm^{-1} of **Q′₂GaOOCC≡CCOOGaQ′₂** complex, probably due to the

tension of the rigid structure. The typical quinaldinate bands profile is checked between 1610 cm^{-1} to 1114 cm^{-1}. Because of the low solubility in the common organic solvents, **Q′$_2$GaOOCC≡CCOOGaQ′$_2$** complex wasn't possible to record the ^{1}H NMR spectra. While the spectral profile and the protons number of **Q′$_2$GaOOC(CH$_2$)$_{12}$COOGaQ′$_2$** complex confirm its chemical structure.

5.7 Multimetallic Gallium complexes obtained with polycarboxylate ligand

The previous synthesis of bimetallic compounds was a preliminary study to understand the possibility to obtain a multimetallic complex as described in Paragraph 5.3 but choosing a ligand with four carboxylic acids as [4,4′,4′′,3′′′-(21*H*,23*H*-porphine-5,10,15,20 tetrayl tetrakis-(benzoic acid)] **H$_2$TTP(COOH)$_4$** illustrated in **Figure 5.21**.

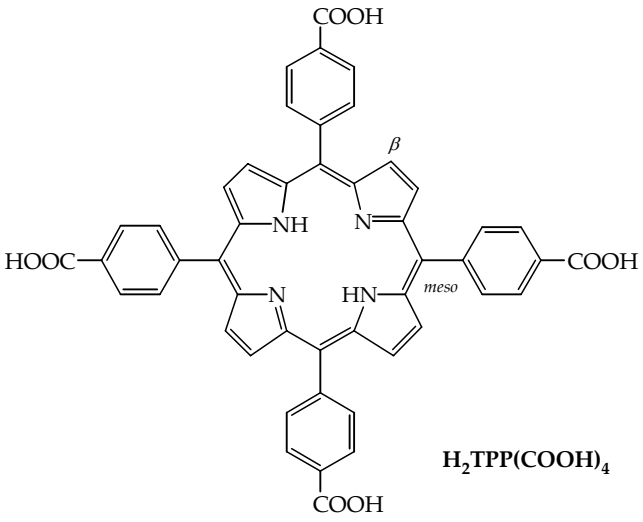

Figure 5.21: H$_2$TTP(COOH)$_4$.

The synthesis was performed in two steps following exactly the same procedure previously described and reported in **Scheme 5.15**.

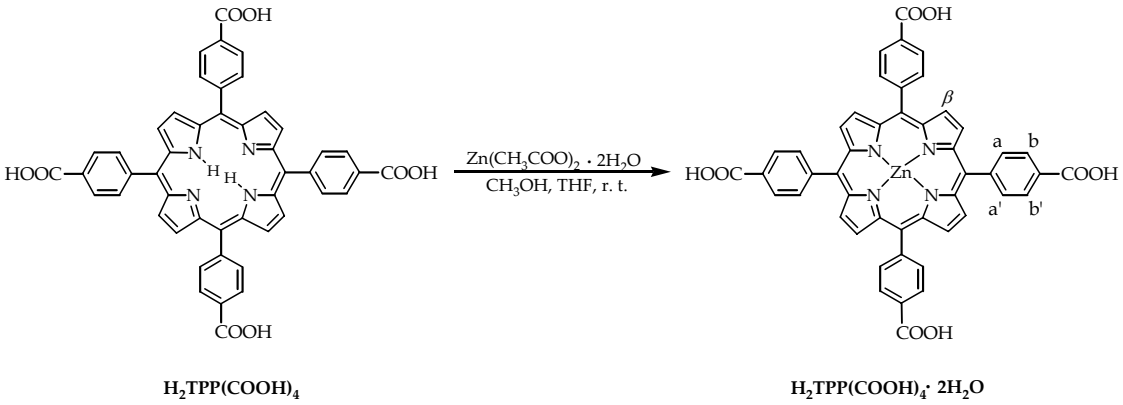

Scheme 5.15: *synthetic procedure for ZnTPP(COOH)4.*

H2TTP(COOH)4 revealed lower solubility than **H2TTP(OH)4** in tetrahydrofurane. After the methanolic solution of zinc acetate dihydrate was added to the reaction mixture suddenly its colour changed in dark violet. The **ZnTPP(COOH)4** was obtained as a dark violet precipitated in the reaction mixture. The product was filtered, washed with water, ethanol and diethyl ether to obtain very good reaction yields. IR spectra shows the broad band of the carboxylic stretching at 3125 cm^{-1}, the C=O stretching was observed at 1703 cm^{-1} at lower frequencies respect to the free porphyrin.

The presence of a new intense band at 1404 cm^{-1} was evidenced. But the elemental analysis are in disagreement with the theoretical values, probably due also to the hygroscopicity of the porphirinic carboxylic functions. Because of the poor solubility wasn't possible to register ^1H NMR spectra.

ZnTPP(COOH)4 compound was activated with NaOH in ethanol in 1:4 molar ratio, and successively dropped in an aqueous solution of gallium(III) nitrate hydrate, finally an ethanolic solution of 2-methyl-8-hydroxyquinoline was added to the reaction mixture with **ZnTPP(COOH)4**: Ga:HQ' in 1:4:8 molar ratio as illustrated in **Scheme 5.16**.

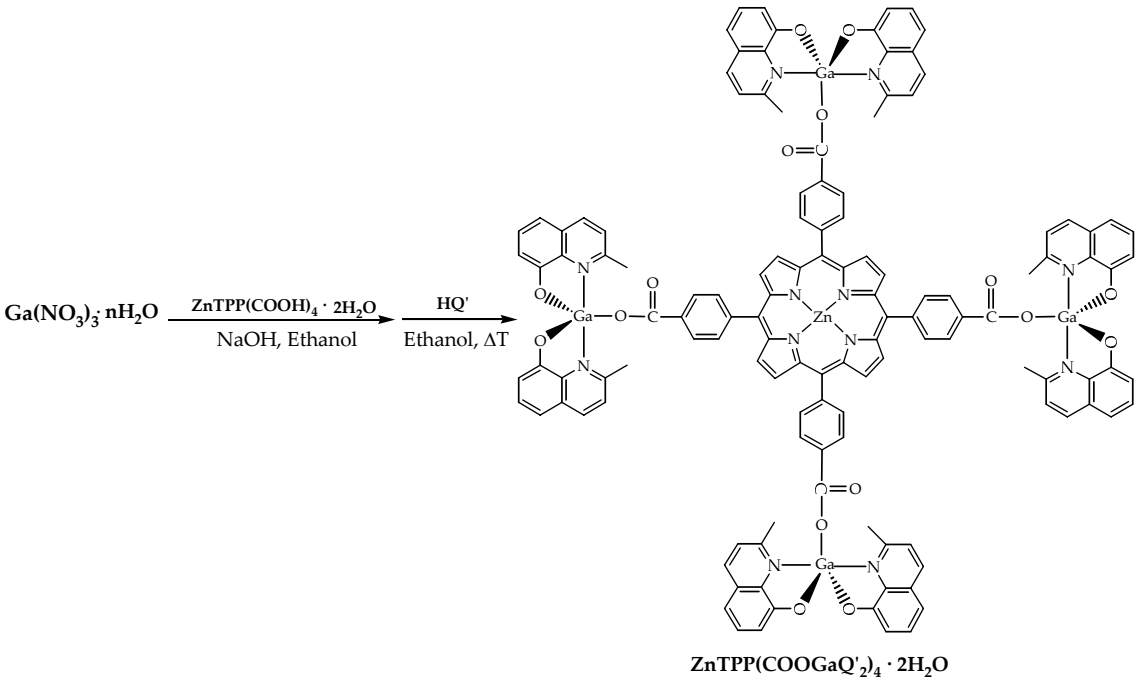

Scheme 5.16: *reaction procedure of* ***ZnTPP(COOGaQ$_2$')$_4$.***

The **ZnTPP(COOGaQ$_2$')$_4$** compound was obtained as brown solid with 60% reaction yield, its purity is confirmed by elemental analysis. Further the IR spectra reveals the C=O stretching band at 1715 cm^{-1} and the typical quinolinate bands profile. Unlikely the poor solubility of this compound, the ^{1}H NMR spectra were not collected, but due to this chemical feature probably the purification from the *GaQ'$_3$* impurity was allowed.

5.8 Conclusions

New bis(2-methyl-8-hydroxyquinolinate) gallium(III) compounds in which the pentacoordination is achieved with a phenoxyde or a carboxylate ligand were synthesised.

5.8.1 Monometallic pentacoordinated synthesised with monodentate ligand

Pentacoordinated compounds with the general formula **Q′$_2$GaL^n**, as illustrated in **Figure 5.1**, where obtained as yellow greenish powder in good reaction yields at list 50% showing good solubility in chloroform. The thermal behaviour reveal high melting point and the absence of polymorphism. X-ray diffraction data were collected on single crystals obtained for slow diffusion of *n*-hexane in chloroform solution. The angles around the Ga(III) ion confirm a trigonal bipyramid geometry and the presence of a –CN and –NO_2 group in the phenol *p*-position influence the crystal system of these compounds. **Q′$_2$GaOC$_6$H$_5$** complex crystallize in monoclinic space group while the **Q′$_2$GaOC$_6$H$_4$CN** and **Q′$_2$GaOC$_6$H$_4$NO$_2$** complexes crystallize in the triclinic being these complexes isostructurals. In all cases, both the Q′ ligands (named Q′$_A$ and Q′$_B$) are involved in aromatic interactions with the symmetrical related rings, while stacks with mixed chelates are not found. Intermolecular π–π stacking interactions mainly involve the pyridyl–pyridyl rings of neighbouring molecules. The π–π stacking is confirmed by the primary motif between the planar aromatic units for both chelates as offset face-to-face (OFF) type. While the phenol rings are involved in edge-to-face interactions (EF), referred as C–H–π hydrogen bonds, being the aromatic ring H donor in the case of complex **Q′$_2$GaOC$_6$H$_5$** and H acceptor in both complexes **Q′$_2$GaOC$_6$H$_4$CN** and **Q′$_2$GaOC$_6$H$_4$NO$_2$**.

The crystal packing reveals that the Q′$_A$–Q′$_A$ stacking is characterized by the same parameters in the series of these gallium compounds, the Q′$_B$–Q′$_B$ aromatic interaction differs from complex **Q′$_2$GaOC$_6$H$_5$** to complexes **Q′$_2$GaOC$_6$H$_4$CN** and **Q′$_2$GaOC$_6$H$_4$NO$_2$**. These feature revealed in the secondary motif may influence the nature of charge transport properties of these materials. The chemical reactivity of the carboxylate derivatives toward gallium(III) cation allowed the synthesis of new bisquinaldinated gallium compounds, with the

general formula **Q'$_2$GaL'$_n$** as illustrated in **Figure 5.10** and **Figure 5.13**. The synthesis was performed choosing *p*-substituted and trisubstituted benzoic acids derivatives as monodentate ligands. All compounds obtained with *p*-substituted benzoic acids derivatives were collected in good reaction yields, noteworthy the gallium compound synthesised with *p*-octyloxybenzoate was obtained by substitution reaction of the phenoxyde ligand in the coordination sphere of **Q'$_2$GaOC$_4$H$_5$** compound, demostrating the strong chemical affinity between gallium(III) and carboxylates. All complexes show good solubility in chloroform, the presence of aliphatic chains in the molecular structure influence the melting point decrease. Crystallographic data collected single crystal for **Q'$_2$GaOOCC$_6$H$_4$O(CH$_2$)$_5$CH$_3$** compound confirm the trigonal bipyramid geometry and pyridyl-pyridyl stacking between quinolinate moieties of two adjacent molecules.

Compounds obtained with trisubstituted benzoic acids were synthesised. Because of the solubility features of the monodentate ligand the reaction yield were quite low, but the presence of three aliphatic chains in the molecular structure extend the solubility of the gallium compounds also in diethyl ether and petroleum ether. Further the mesogen properties an the crystallographic data of **Q'$_2$GaOOCC$_6$H$_2$(OC$_{14}$H$_{29}$)$_3$** compound are still under investigation.

5.8.2 Bimetallic compounds with biphenol and bicarboxylic acids derivatives

The good chemical affinity between gallium(III) and phenoxydes derivatives was exploited to synthesis bimetallic pentacoordinated compounds. Only **Q'$_2$GaOC$_6$H$_4$C$_6$H$_4$OGaQ'$_2$**, showed in **Scheme 5.2**, was collected as pure light green powder.

Two *Q'2Ga-* fragment are linked together with a rigid aromatic ligand. Bimetallic pentacoordinated gallium compound where the linker is a biphenol

are unknown in literature. Unlikely this complex show very low solubility to be applied in solution–based methods in OLED fabrication technologies.
Instead the synthesis of bimetallic compounds obtained with bicarboxylic acids as a flexible or rigid insature ligands linking two *Q'2Ga-* fragments give the green complexes **Q'$_2$GaOOC(CH$_{12}$)COOGaQ'$_2$** and **Q'$_2$GaOOCC≡CCOOGaQ'$_2$**, **Scheme 5.14**, solubles in chloroform.

5.8.3 Polymetallic gallium compounds

The possibility to obtain bimetallic compound with biphenols and bicarboxylic acids suggested to synthesis polymetallic compounds using porphyrin derivatives bearing phenols and carboxylic acids in *meso* positions. So four *Q'$_2$Ga-* fragments in peripheral position and a metal cation as zinc in the porphyrinic core were introduced in the same structure. For that reason **H$_2$TPP(OH)$_4$** and **H$_2$TPP(COOH)$_4$** porphyrins were chosen as rigid extended heteroaromatic macrocycle. Then the synthesis of **ZnTPP(OGaQ'$_2$)$_4$** and **ZnTPP(COOGaQ'$_2$)$_4$** compounds (**Scheme 5.5** and **Scheme 5.16** respectively) was performed in two steps. The obtained compounds show differences in the aspect and in the solubility, so **ZnTPP(COOGaQ'$_2$)$_4$** is a brown insoluble powder while **ZnTPP(OGaQ'$_2$)$_4$**, dark blue solid, is soluble in methanol allowing further characterisations.
^{1}H NMR spectra and the elemental analysis not allowed to distinguish if the resulting data were due to a single compound or to the contribution of a mixture of polymetallic species as **ZnTPP(OH)$_3$(OGaQ'$_2$)**, **ZnTPP(OH)$_2$(OGaQ'$_2$)$_2$**, or **ZnTPP(OH)(OGaQ'$_2$)$_3$** that were also synthesised in order to understand the chemical behaviour of this kind of systems. The MALDI/TOF mass spectrometry confirm the presence of **ZnTPP(OGaQ'$_2$)$_4$** as main product but traces of the homologous polymetallic species (Ga$_3$/Zn,

Ga_2/Zn or Ga/Zn) which usually form together with Ga_4/Zn, were detected. In order to overcome this problem a different synthetic pathway was performed, but insoluble products were obtained so their characterization wasn't permitted. The experimental evidence of **ZnTPP(OGaQ'$_2$)$_4$** heterobimetallic compound was obtained. This complex is a test compound to study synthetic pathway to introduce more *Q'$_2$Ga-* chromophores in the same structure.

REFERENCES

1. Sapochak, L. S.; Burrows, P. E.; D. Garbuzov, D. M. Ho, S. R. Forrest, M. E. Thompson, *J. Phys. Chem.* **1996**, *100*, 17766.

2. Schmidbaur, H.; Lettenbauer, J.; Wilkinson, D. L.; Muller, G.; Kumberger, O. *Z. Naturforsh.* **1991**, *46b*, 901.

3. US Patent 6.503.643, **2003**.

4. EP Patent 0 757 088 A2, **1997**.

5. Elschner, A.; Heuer, H. W.; Jonas, F.; Kirchmeyer, S.; Wehrmann, R.; Wussow, K. *Adv. Mater.* **2001**, *13*, 1811.

6. Shiro, M.; Fernando, Q. *Anal. Chem.* **1971**, *43*, 10, 1222.

7. Baldo, M. A.; O'Brien, D. F.; You, Y.; Shoustikov, A., Sibley, S.; Thompson M. E.; Forrest, S.R. *Nature* **1998**, *395*, 151.

8. Scandola, F.; Chiorboli, C.; Prodi, A.; Iengo, E; Alessio, E. *Coord. Chem. Rev.* **2006**, *250*, 1471. Anderson, H. L. *Chem. Commun.* **1999**, 2323.

9. Rowley, N. M.; Kurek, S. S.; Foulon, J.-D.; Hamor, T. A.; Jones, J. J.; McCleverty, J. A.; Hubig, S. M.; mcInnes, E. J. L.; Payne, N. N.; Yellowlees, L. J. *Inorg. Chem.* **1995**, *34*, 4414.

10. La Deda, M.; Ghedini, M.; Aiello, I.; De Franco, I. *Inorg. Chem. Commun.* **2004**, *7*, 1273.

11. Aiello, I.; Di Donna, L.; Ghedini, M.; La Deda, M.; Napoli, A.; Sindona, G. *Anal. Chem.* **2004**, *76*, 20, 5985.

12. Binnemans, K.; Lodewyckx, K.; Cardinaels, T.; Parac-Vogt, T.; Bourgogne, C.; Guillon D.; Donnio, B. *Eur. J. Chem.* **2006**, 150.

13. Bondzic, S.; de Wit, J.; Polushkin, E.; Schouten, A. J.; ten Brinke, G.; Ruokolainen, J.; Ikkala, O.; Dolbnya, I.; Bras, W. *Macromolecules* **2004**, *37*, 9517.